International Journal of Vehicle Design

ISSN online: 1741-5314 - ISSN print: 0143-3369
https://www.inderscience.com/ijvd

Dual-redundancy multi-mode control of high safety reliability steering wheel system

Mi Junnan, Wang Tong, Lian Xiaomin

DOI: 10.1504/IJVD.2024.10061811

Article History:

Received:	04 October 2020
Accepted:	16 May 2021
Published online:	23 January 2024

Dual-redundancy multi-mode control of high safety reliability steering wheel system

Mi Junnan, Wang Tong and Lian Xiaomin*

School of Vehicle and Mobility,
Tsinghua University,
Beijing, 100084, China
Email: thumjn@163.com
Email: wangtong19929@foxmail.com
Email: lianxm@tsinghua.edu.cn
*Corresponding author

Abstract: The steering wheel system of a steer-by-wire system (SBW) offers steering torque to the driver. In order to improve its safety and reliability, a dual-redundancy steering wheel system has been proposed by some research. This research proposes a dual-redundancy multi-mode control method for this system, which is divided into different control modes, namely the angle alignment mode, the pivot steer with resistance mode and the uniform approaching to middle position mode, so that the system can adapt to different vehicle running states and driver's manipulation habits. At the same time, a torque balance control method for two channel motors is proposed to balance their torques and an order-reduce and reforming control method is proposed so that the system can still work even one motor fails. Finally, this study built a vehicle test platform to verify the control method and prove its effectiveness.

Keywords: steer-by-wire; safety; steering wheel; redundancy; control; steering torque; SBW.

Reference to this paper should be made as follows: Junnan, M., Tong, W. and Xiaomin, L. (2024) 'Dual-redundancy multi-mode control of high safety reliability steering wheel system', *Int. J. Vehicle Design*, Vol. 94, Nos. 1/2, pp.1–37.

Biographical notes: Mi Junnan graduated from Tsinghua University with a Bachelor's degree in Vehicle Engineering in 2015. He graduated from the School of Vehicle and Mobility at Tsinghua University in 2021 with a PhD in Engineering. His research direction is automotive steer-by-wire system control.

Wang Tong graduated from Tsinghua University with a Bachelor's degree in Vehicle Engineering in 2014. She graduated from the School of Vehicle and Mobility at Tsinghua University in 2020 with a PhD in Engineering. Her research direction is the functional safety of automotive steer-by-wire system and its architecture design.

Lian Xiaomin is a Professor at Tsinghua University, a member of the Chinese Society of Automotive Engineering, the Director of the Institute of Automotive Electronics at the School of Vehicles and Transportation at Tsinghua University, and the Deputy Director of the Institute of Transportation at Tsinghua University. Her main research direction is automotive electronic control, automotive dynamic measurement and control theory and technology.

1 Introduction

A steer-by-wire system (SBW) is a vehicle steering system, in which the mechanical connection between the steering wheel and the steering gear in the traditional mechanical steering system is removed. A steering wheel system is installed under the steering wheel to provide steering torque and a steering motor is installed on the steering gear to drive the steering actuator.

The torque on the steering wheel is necessary while driving (Balachandran and Gerdes, 2015). It can offer the feeling of middle position to driver. Meanwhile, a sudden disappearance of steering torque may lead to steering misoperation for the hysteresis of driver reaction. Moreover, the driver safety will be in great danger if the driver releases the steering wheel habitually after turning while a loss of steering torque occurs, because the car will continue turning rather than restoring straight running state. A serious accident may be caused by the unexpected vehicle behaviour.

As mentioned above, the high safety reliability is necessary for steering wheel system. In a common SBW, the steering wheel system is a single redundancy electromechanically coupled system. The reliability of its electronic part is insufficient for the requirement of ASIL-D level in ISO-26262 (Wang et al., 2018). Once a failure of electronic components occurs, the steering torque may be lost for the lack of a backup part. In addition, the failure occurs with no warning, which means the driver does not have enough preparation time for the loss of steering torque.

Regarding the problem of insufficient system safety, many current researches on improving the safety of SBW can be used for reference. Some researches focus on the high safety structure of the system. Huang et al. (2020) analysed the safety and reliability requirements of SBW and proposed a SBW with fail-operational characteristics. In the system structure, only the steering gear is redundant and the safety of the steering wheel system is not considered. Wang et al. (2017, 2018) proposed a quantitative analysis method for the safety and reliability of the dual-redundancy E/E system and proposed a whole dual-redundancy steering wheel system structure. The structure has high safety and reliability. However, in the controller part of this structure, the power supply of one motor may be cut off by the fault controller in another control channel, which will lead to the failure of the entire system. There are some studies (Xu et al., 2018; Zhang and Zhao, 2018; Anwar and Niu, 2014) aiming at the high safety of sensors, which have conducted researches on redundancy and fault tolerance. These studies are of great value to the sensor structure of the system studied in this paper. Some studies are focused on fault-tolerant control of motors in the system. Huang et al. (2020) and Lei et al. (2011) proposed diagnosis methods for motor faults, which compensates and controls the current when the motor has not completely failed. However, these methods cannot solve the system failure problem in the case of complete motor failure. There are also some studies using dual motors in the system to improve the safety. Zou and Zhao (2020) used a dual-motor structure for the steering gear and proposed a dual-motor speed synchronisation control structure. This control method has reference value for the control of the steering wheel system. He et al. (2015) used dual motors to control the steering gear system. One motor performs angle closed-loop control and the other motor follows the target current of the previous motor. With this structure, the currents of the two motors are out of control for a short period of time after the motor of the angle closed-loop control motor fails, which may lead to system instability.

In addition to safety issues, steering control must also consider steering torque control issues. This problem has been noticed by many studies. Some researches (Cheon and Nam, 2017; Kim and Chu, 2016; Lee et al., 2020; Ma et al., 2016; Zheng et al., 2011, 2013) established dynamic models of the vehicle system or mechanical steering system to simulate its steering torque on the steering wheel. The purpose of these studies is to generate a steering torque close to that of a mechanical steering system. Some studies (Balachandran and Gerdes, 2015; Hayama et al., 2010) set a number of variable parameters in the model after designing the steering torque according to the model and studied the influence of the change of the parameters on the steering torque. According to the traditional mechanical steering system model, Fankem and Müller (2014) divides the steering torque into main torque, friction torque, damping torque, inertia torque and active return torque and sums up the various parts to obtain the steering torque. This method takes into account the situation of active return, which has important reference value.

It can be concluded that there are relatively few researches on the steering wheel system safety and the main reference is the high-safety control method on the steering gear. To solve the problem of the disappearance of steering torque when the motor fails, the dual-motor control method has a higher reference value. Regarding the control of steering torque, most researches focus on system modelling, so that the torque is close to the mechanical system torque. The main problem of these methods is that high accuracy of model parameters is required. At the same time, the different steering habits of driver under different driving conditions and the steering wheel angle control if driver releases the hand have not been studied.

The following will introduce the dual-redundancy multi-mode control method for high safety reliability steering wheel system. First the structure of the high safety reliability steering wheel system is introduced followed by the dual redundancy multi-mode control method. Next is the introduction of the vehicle test results. Finally the conclusion of this paper.

2 Structure of high safety reliability steering wheel system

By applying the redundancy theory to structure design, a dual-redundancy steering wheel system (Junnan et al., 2020) with high safety reliability is proposed, as is shown in Figure 1.

In Figure 1, two angle sensors are put on the steering column to measure the steering wheel angle, of which the angle signals θ_1 and θ_2 are transmitted to the two motor controllers $\mathbf{E}_1$ and $\mathbf{E}_2$. $\mathbf{E}_1$ and $\mathbf{E}_2$ control two motors by sending target currents i_{1t} and i_{2t} to the motor drivers $\mathbf{D}_1$ and $\mathbf{D}_2$. The currents in two motors are controlled by $\mathbf{D}_1$ and $\mathbf{D}_2$ to track their targets respectively, which are i_1 and i_2. Two motors $\mathbf{M}_1$ and $\mathbf{M}_2$ actuate the steering wheel simultaneously by a pair of meshing gears. $\mathbf{L}$ is a mechanical angle limitation stopper on the axle to limit the maximum steering wheel angle with multi-turn spiral mechanism. In addition, two electronic relays are on the power cables of motor drivers $\mathbf{D}_1$ and $\mathbf{D}_2$. The first one is controlled by $\mathbf{E}_2$ and $\mathbf{E}_3$ through the cutting signals c_{21} and c_{31}, and the second one by $\mathbf{E}_1$ and $\mathbf{E}_3$ through the cutting signals c_{12} and c_{32}. During the system operation, three controllers monitor the system simultaneously by collecting signals through sensors and messages on the dual-redundancy network. If a

failure occurs, at least two of the three controllers can identify the fault. In some cases, the control of two motors can be performed even a fault occurs, such as a failure of angle sensor or a network failure. However, if a fault occurs in components related to motor control, such as controllers, drivers or motors, the power supply of corresponding driver $\mathbf{D}_1$ or $\mathbf{D}_2$ should be cut off by the other two controllers. For the description of the monitoring of system faults and the cut-off of faulty motors, please refer to Wang et al. (2017).

Figure 1 Structure of SBW with a high safety reliability steering wheel system

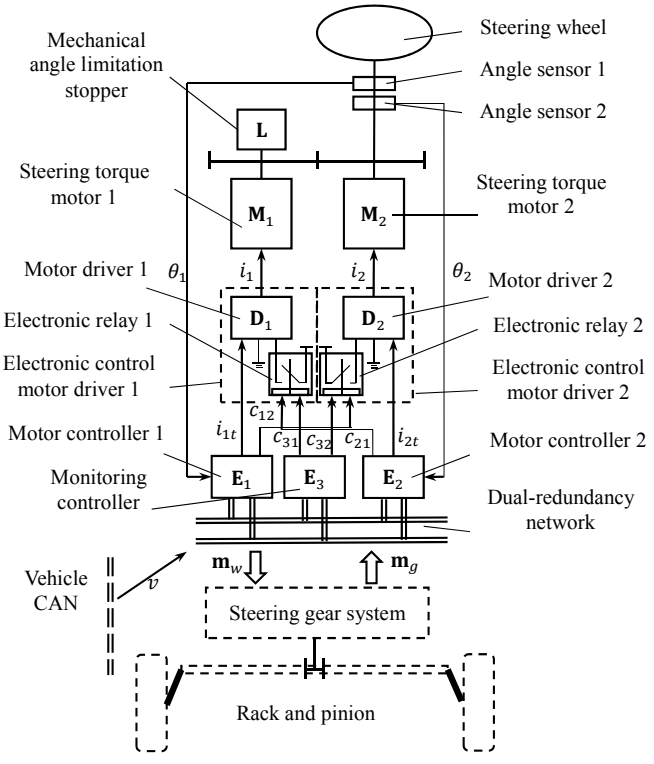

In steering operation, the steering gear system turns the front wheels to track steering wheel angle. Thus the steering wheel angle signal θ_w is transmitted to the steering gear system through dual-redundancy network. In addition, a control mode flag j is sent as well, which will be described in detail in Section 3.2. Steering wheel angle signal θ_w and control mode flag j make up the vector signal $\mathbf{m}_w$, as is shown in equation (1).

$$\mathbf{m}_w = \{\theta_w, j\} \tag{1}$$

At the same time, steering gear system needs to send the messages the steering wheel system requires- $\mathbf{m}_g$ -to dual-redundancy network, which included the steering wheel target angle θ_{wt} and steering motor current i_g, as in equation (2).

$$\mathbf{m}_g = \{\theta_{wt}, i_g\} \tag{2}$$

Steering wheel system and steering gear system operate coordinately by sending messages to each other.

Moreover, vehicle speed message v is sent to steering wheel from vehicle CAN through the dual-redundancy network as the working of steering wheel is relevant to vehicle speed.

The control method of steering wheel system will be described in detail below.

3 Dual-redundancy multi-mode control strategy

The characteristics of system dual-redundancy need to be considered in control. The two control channels, each of which contains a controller, a driver and a motor, work coordinately when no fault occurs. The torques of two motors should keep balance in this working state. If a fault occurs and the power supply of one motor is cut by the other two controllers, the remaining motor should take over all torque output and continue controlling the steering wheel. The control of two motors in no-fault state and one motor in one-fault state is dual-redundancy control.

The driver's steering wheel operation requirements are different according to different vehicle speeds. When the car is parked, the drivers needs to feel resistance as the steering wheel is turning. The steering wheel should stay still if released. If the car is running, driver should feel the aligning torque while holding the steering wheel and the steering wheel can return to middle position after released. Therefore, the control of steering wheel system should vary according to the different vehicle speeds, which means its control requires multiple modes.

The block diagram of dual-redundancy multi-mode control is shown in Figure 2.

As is shown in Figure 2, vehicle speed v and vector signal from steering gear system $\mathbf{m}_g$ are transmitted to two multi-mode control blocks 'Multi-mode control 1' and 'Multi-mode control 2' simultaneously. The steering wheel target angle θ_{wt} in $\mathbf{m}_g$ and vehicle speed v are sent to two mode estimation blocks. $\mathbf{F}$ is dual-redundancy management block, of which the functions are fusing the angle signals of two angle sensors θ_1 and θ_2 into actual angle θ_w, monitoring the system operation status, determining whether the system is malfunctioning and transmitting signals c_{21}, c_{31}, c_{12} and c_{32} to cut off the power of faulty motor. In the vector signal $\mathbf{m}_f$ sent from $\mathbf{F}$ to two multi-mode control blocks, there are steering wheel actual angle θ_w and cutting signal c as shown in equation (3).

$$\mathbf{m}_f = \{\theta_w, c\} \tag{3}$$

In equation (3), cutting signal c is the signal for the control when a motor power is cut off. It means which one of the two channels is cut. For instance, if the power of electrically drive module 2 is cut off, 'Multi-mode control 1' should adjust its control method according to the cutting signal c.

Figure 2 Dual-redundancy multi-mode control

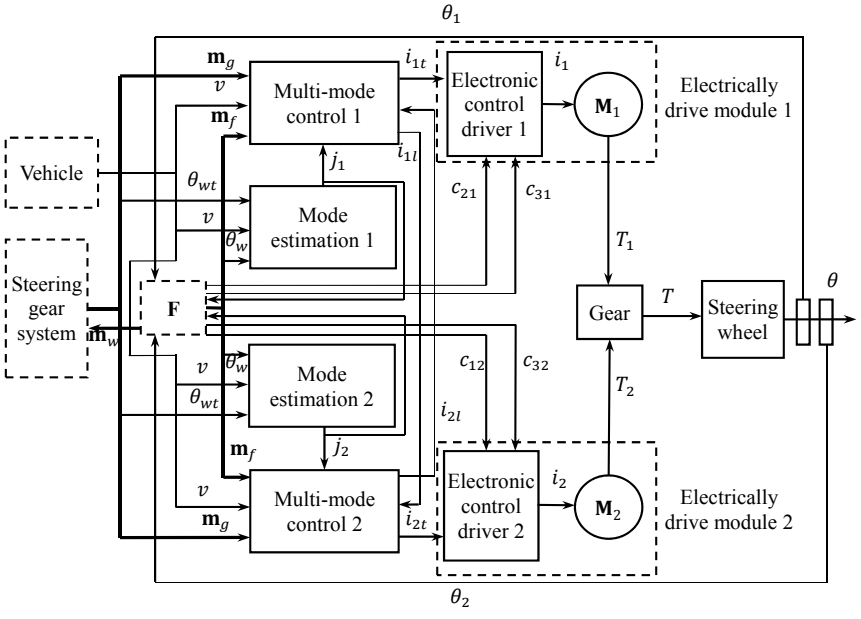

Signal outputs of two mode estimation blocks j_1 and j_2 are sent to **F** to calculate the control mode flag j in equation (1), which represent the different control modes. i_{1l} and i_{2l} are currents sent from one control block to another, which are used for torque balance control that will be described in Section 3.3. i_{1t} and i_{2t} are motor target currents. The torques of two motors T_1 and T_2 act on the gears and the output of gears is the steering torque T. The output of steering wheel is its real physical angle θ, which is measured by dual-redundancy angle sensors.

The above is the overall control architecture of the dual-redundancy multi-mode control of steering wheel system. The control method will be described in detail below.

3.1 Dual-redundancy control analysis of two motors

As shown in Figure 2, two control channel motors work simultaneously to generate steering torque on the steering wheel, which is the most obvious feature of dual-redundancy control. In system working with no-fault condition, the torques of two motors are simultaneously applied to the steering wheel. In order to prolong the service life of the motors and related circuits, their torques should be equal.

In order to perform the balance control of motor torques, the mathematical model of the entire control system will be analysed below.

The actual motor currents follow the targets. Assuming that the following speeds of the currents are much greater than the response speed of the mechanical system, then the actual currents are regarded as equal to the target currents, as shown in equation (4).

$$\begin{cases} i_1 = i_{1t} \\ i_2 = i_{2t} \end{cases} \tag{4}$$

In equation (4), i_{1t} and i_{2t} are target currents of two motors, i_1 and i_2 are actual currents.

The system dynamic equation is shown in equation (5).

$$J\ddot{\theta}_w + B\dot{\theta}_w + T_f = \left(i_{1t} + i_{2t}\right) K_T \varphi + T_h \tag{5}$$

In equation (5), K_T is the motor torque coefficient, φ is the mechanical efficiency of gears, J is the system mechanical inertia, B is damping coefficient and T_f is the resistance moment. $\dot{\theta}_w$ and $\ddot{\theta}_w$ are the angular velocity and angular acceleration of the steering wheel. T_h is the torque applied by the driver to the steering wheel. The motor torques drive the steering wheel to rotate together with the steering torque of the driver.

Rewrite the above kinetic equation as a state space equation, as shown in equation (6).

$$\begin{cases} \dot{\mathbf{X}}_1 = \begin{bmatrix} 0 & 1 \\ 0 & -\dfrac{B}{J} \end{bmatrix} \mathbf{X}_1 + \begin{bmatrix} 0 & 0 \\ \dfrac{K_T\varphi}{J} & \dfrac{K_T\varphi}{J} \end{bmatrix} \mathbf{u}_1 + \begin{bmatrix} 0 \\ \dfrac{T_h - T_f}{J} \end{bmatrix} \\ y = \begin{bmatrix} 1 & 0 \end{bmatrix} \mathbf{X}_1 \end{cases} \tag{6}$$

The meanings of state matrix $\mathbf{X}_1$ and input matrix $\mathbf{u}_1$ are shown in equation (7).

$$\mathbf{X}_1 = \begin{bmatrix} \theta_w \\ \dot{\theta}_w \end{bmatrix}, \mathbf{u}_1 = \begin{bmatrix} i_{1t} \\ i_{2t} \end{bmatrix} \tag{7}$$

Rewrite equation (6) into the following form.

$$\begin{cases} \dot{\mathbf{X}}_1 = \mathbf{A}_1 \mathbf{X}_1 + \mathbf{B}_1 \mathbf{u}_1 + w \\ y = \mathbf{C}_1 \mathbf{X}_1 \end{cases} \tag{8}$$

The meanings of system matrix $\mathbf{A}_1$, input matrix $\mathbf{B}_1$, interference $\mathbf{w}$ and output matrix $\mathbf{C}_1$ are shown in equation (9).

$$\mathbf{A}_1 = \begin{bmatrix} 0 & 1 \\ 0 & -\dfrac{B}{J} \end{bmatrix}, \mathbf{B}_1 = \begin{bmatrix} 0 & 0 \\ \dfrac{K_T\varphi}{J} & \dfrac{K_T\varphi}{J} \end{bmatrix}, \mathbf{w} = \begin{bmatrix} 0 \\ \dfrac{T_h - T_f}{J} \end{bmatrix}, \mathbf{C}_1 = \begin{bmatrix} 1 & 0 \end{bmatrix} \tag{9}$$

The block diagram of the above system kinetic state space description is shown in Figure 3.

Figure 3 System kinetic state space description block diagram

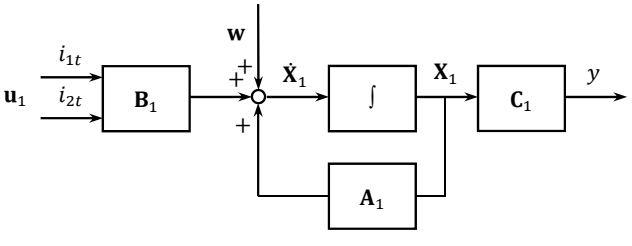

The meaning of each symbol in Figure 3 corresponds to that in equation (8).

The controllability matrix of the system above $\mathbf{Q}_k$ is shown in equation (10).

$$\mathbf{Q}_k = \begin{bmatrix} 0 & 0 & \dfrac{K_T\varphi}{J} & \dfrac{K_T\varphi}{J} \\ \dfrac{K_T\varphi}{J} & \dfrac{K_T\varphi}{J} & -\dfrac{BK_T\varphi}{J^2} & -\dfrac{BK_T\varphi}{J^2} \end{bmatrix} \tag{10}$$

The rank of $\mathbf{Q}_k$ is equal to 2, showing that the mechatronic system is fully controllable.

A dual-redundancy closed-loop control structure is required in order to control the mechatronics system as shown in Figure 4.

Figure 4 Dual-redundancy closed-loop control structure

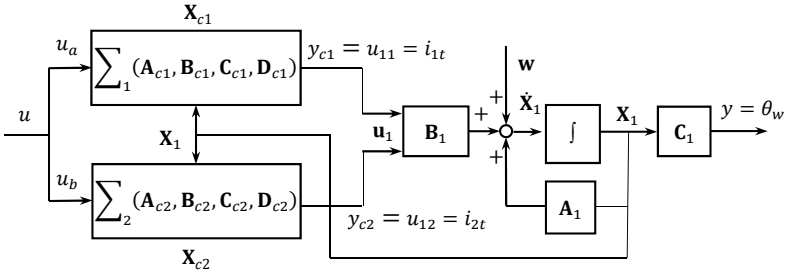

In Figure 4, $\sum_1(\mathbf{A}_{c1},\mathbf{B}_{c1},\mathbf{C}_{c1},\mathbf{D}_{c1})$ and $\sum_2(\mathbf{A}_{c2},\mathbf{B}_{c2},\mathbf{C}_{c2},\mathbf{D}_{c2})$ are dual-redundancy controllers, of which the reference inputs are u_a and u_b. The two reference inputs u_a and u_b are theoretically equal to reference input u. In addition, the state matrix $\mathbf{X}_1$ is the feedback of the closed-loop control. $\mathbf{X}_{c1}$ and $\mathbf{X}_{c2}$ are state matrixes of two controllers. The outputs of two controllers are y_{c1} and y_{c2}, which form the input vector of the mechatronics system $\mathbf{u}_1$. The other parts in Figure 4 is the mechatronic system introduced in Figure 3.

The state space equation of dual-redundancy controllers $\sum_1(\mathbf{A}_{c1},\mathbf{B}_{c1},\mathbf{C}_{c1},\mathbf{D}_{c1})$ and $\sum_2(\mathbf{A}_{c2},\mathbf{B}_{c2},\mathbf{C}_{c2},\mathbf{D}_{c2})$ are shown in equations (11) and (12)

$$\sum_1 : \begin{cases} \dot{\mathbf{X}}_{c1} = \mathbf{A}_{c1}\mathbf{X}_{c1} + \mathbf{B}_{c1}\begin{bmatrix} u_a \\ \mathbf{X}_1 \end{bmatrix} \\ y_{c1} = \mathbf{C}_{c1}\mathbf{X}_{c1} + \mathbf{D}_{c1}\begin{bmatrix} u_a \\ \mathbf{X}_1 \end{bmatrix} \end{cases} \tag{11}$$

$$\sum_2 : \begin{cases} \dot{\mathbf{X}}_{c2} = \mathbf{A}_{c2}\mathbf{X}_{c2} + \mathbf{B}_{c2}\begin{bmatrix} u_b \\ \mathbf{X}_1 \end{bmatrix} \\ y_{c2} = \mathbf{C}_{c2}\mathbf{X}_{c2} + \mathbf{D}_{c2}\begin{bmatrix} u_b \\ \mathbf{X}_1 \end{bmatrix} \end{cases} \tag{12}$$

As shown in equations (11) and (12), their outputs together form the input vector $\mathbf{u}_1$ as shown in equation (13).

$$\mathbf{u}_1 = \begin{bmatrix} i_{1t} \\ i_{2t} \end{bmatrix} = \begin{bmatrix} y_{c1} \\ y_{c2} \end{bmatrix} \tag{13}$$

Differentiate equation (13) and substitute the state equations of equations (11) and (12) into it, equation (14) can be obtained.

$$\dot{\mathbf{u}}_1 = \begin{bmatrix} \dot{y}_{c1} \\ \dot{y}_{c2} \end{bmatrix} = \begin{bmatrix} \mathbf{C}_{c1}\dot{\mathbf{X}}_{c1} + \mathbf{D}_{c1}\begin{bmatrix} \dot{u}_a \\ \dot{\mathbf{X}}_1 \end{bmatrix} \\ \mathbf{C}_{c2}\dot{\mathbf{X}}_{c2} + \mathbf{D}_{c2}\begin{bmatrix} \dot{u}_b \\ \dot{\mathbf{X}}_1 \end{bmatrix} \end{bmatrix} = \begin{bmatrix} \mathbf{C}_{c1}\left(\mathbf{A}_{c1}\mathbf{X}_{c1} + \mathbf{B}_{c1}\begin{bmatrix} u_a \\ \mathbf{X}_1 \end{bmatrix}\right) + \mathbf{D}_{c1}\begin{bmatrix} \dot{u}_a \\ \dot{\mathbf{X}}_1 \end{bmatrix} \\ \mathbf{C}_{c2}\left(\mathbf{A}_{c2}\mathbf{X}_{c2} + \mathbf{B}_{c2}\begin{bmatrix} u_b \\ \mathbf{X}_1 \end{bmatrix}\right) + \mathbf{D}_{c2}\begin{bmatrix} \dot{u}_b \\ \dot{\mathbf{X}}_1 \end{bmatrix} \end{bmatrix} \tag{14}$$

Decompose matrix $\mathbf{B}_{c1}$ and $\mathbf{D}_{c1}$ in equation (14) into two parts, as shown in equations (15) and (16).

$$\begin{cases} \mathbf{B}_{c1} = \begin{bmatrix} \mathbf{B}_{c11} & \mathbf{B}_{c12} \end{bmatrix} \\ \mathbf{B}_{c2} = \begin{bmatrix} \mathbf{B}_{c21} & \mathbf{B}_{c22} \end{bmatrix} \end{cases} \tag{15}$$

$$\begin{cases} \mathbf{D}_{c1} = \begin{bmatrix} d_{c11} & \mathbf{D}_{c12} \end{bmatrix} \\ \mathbf{D}_{c2} = \begin{bmatrix} d_{c21} & \mathbf{D}_{c22} \end{bmatrix} \end{cases} \tag{16}$$

Substituting equations (15) and (16) into equation (14), the simplified result is shown in equation (17).

$$\dot{\mathbf{u}}_1 = \begin{bmatrix} \mathbf{C}_{c1}\left(\mathbf{A}_{c1}\mathbf{X}_{c1} + \begin{bmatrix} \mathbf{B}_{c11} & \mathbf{B}_{c12} \end{bmatrix}\begin{bmatrix} u_a \\ \mathbf{X}_1 \end{bmatrix}\right) + \begin{bmatrix} d_{c11} & \mathbf{D}_{c12} \end{bmatrix}\begin{bmatrix} \dot{u}_a \\ \dot{\mathbf{X}}_1 \end{bmatrix} \\ \mathbf{C}_{c2}\left(\mathbf{A}_{c2}\mathbf{X}_{c2} + \begin{bmatrix} \mathbf{B}_{c21} & \mathbf{B}_{c22} \end{bmatrix}\begin{bmatrix} u_b \\ \mathbf{X}_1 \end{bmatrix}\right) + \begin{bmatrix} d_{c21} & \mathbf{D}_{c22} \end{bmatrix}\begin{bmatrix} \dot{u}_b \\ \dot{\mathbf{X}}_1 \end{bmatrix} \end{bmatrix} \tag{17}$$

Write out the two current state components in equation (17), as shown in equation (18).

$$\begin{cases} \dfrac{\mathrm{d}}{\mathrm{d}t} i_{1t} = \mathbf{C}_{c1}\mathbf{B}_{c11}u_a + d_{c11}\dot{u}_a + (\mathbf{C}_{c1}\mathbf{B}_{c12} + \mathbf{D}_{c12}\mathbf{A}_1)\mathbf{X}_1 + \mathbf{D}_{c12}\mathbf{B}_1\begin{bmatrix} i_{1t} \\ i_{2t} \end{bmatrix} \\ \qquad\qquad + \mathbf{C}_{c1}\mathbf{A}_{c1}\mathbf{X}_{c1} + \mathbf{D}_{c12}\mathbf{w} \\ \dfrac{\mathrm{d}}{\mathrm{d}t} i_{2t} = \mathbf{C}_{c2}\mathbf{B}_{c21}u_b + d_{c21}\dot{u}_b + (\mathbf{C}_{c2}\mathbf{B}_{c22} + \mathbf{D}_{c22}\mathbf{A}_1)\mathbf{X}_1 + \mathbf{D}_{c22}\mathbf{B}_1\begin{bmatrix} i_{1t} \\ i_{2t} \end{bmatrix} \\ \qquad\qquad + \mathbf{C}_{c2}\mathbf{A}_{c2}\mathbf{X}_{c2} + \mathbf{D}_{c22}\mathbf{w} \end{cases} \tag{18}$$

To make the torques of two motors equal, their actual currents should be equal under the condition of the same torque coefficient. Assuming that the actual currents can quickly follow the target currents, the target becomes making their target currents equal. According to equation (18), the upper and lower equations need to be equal when the

initial values of target currents are the same. If the two channel reference inputs are equal, that is, when $u_a = u_b$ and $\dot{u}_a = \dot{u}_b$, it is only necessary to make the matrixes of the two controllers, $\sum_1(\mathbf{A}_{c1}, \mathbf{B}_{c1}, \mathbf{C}_{c1}, \mathbf{D}_{c1})$ and $\sum_2(\mathbf{A}_{c2}, \mathbf{B}_{c2}, \mathbf{C}_{c2}, \mathbf{D}_{c2})$, the same, as shown in equation (19).

$$\mathbf{A}_{c1} = \mathbf{A}_{c2}, \mathbf{B}_{c1} = \mathbf{B}_{c2}, \mathbf{C}_{c1} = \mathbf{C}_{c2}, \mathbf{D}_{c1} = \mathbf{D}_{c2} \tag{19}$$

However, due to the communication delay of the two controllers, the values of the inputs u_a and u_b of the two control channels are close, but they may be not equal in the same operation cycle, that is, $u_a \neq u_b$. Furthermore, the differential effect on the reference input causes $\dot{u}_a \neq \dot{u}_b$ and the difference between the two may not be ignored. The difference between the reference inputs and their differential signals will result in the difference of the two current differentials in equation (18), which will destroy the balance of the target currents of the two motors.

When the two controller structures and parameters are the same, in order to solve the problem of unbalanced target currents caused by the different reference inputs, a current balance distribution module is added to the control system. The refactored system control structure is shown in Figure 5.

In Figure 5, a current balance distribution module $\mathbf{T}$ is added between the original two channel controllers and the mechatronics control object. Its inputs are y_{c1} and y_{c2}, the output signals of the original two channel controllers, and the outputs are the target current i_{1t} and i_{2t}.

Figure 5 Refactored dual-redundancy closed-loop control structure

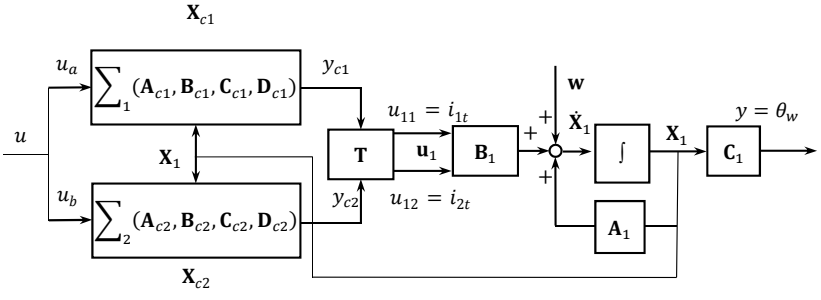

After the calculation of $\mathbf{T}$, the target currents of two motors are shown in equation (20).

$$\mathbf{u}_1 = \mathbf{T}\begin{bmatrix} y_{c1} \\ y_{c2} \end{bmatrix} = \begin{bmatrix} \frac{1}{2} & \frac{1}{2} \\ \frac{1}{2} & \frac{1}{2} \end{bmatrix}\begin{bmatrix} y_{c1} \\ y_{c2} \end{bmatrix} \tag{20}$$

Incorporating equation (20) into equation (17), the state equation of the target currents vector after the balance distribution is obtained, as shown in equation (21).

$$\begin{cases} \dfrac{\mathrm{d}}{\mathrm{d}t} i_{1t} = \mathbf{C}_{c1}\mathbf{B}_{c11}u_a + d_{c11}\dot{u}_a + (\mathbf{C}_{c1}\mathbf{B}_{c12} + \mathbf{D}_{c12}\mathbf{A}_1)\mathbf{X}_1 + \mathbf{D}_{c12}\mathbf{B}_1 \begin{bmatrix} i_{1t} \\ i_{2t} \end{bmatrix} \\ \qquad\qquad + \mathbf{C}_{c1}\mathbf{A}_{c1}\mathbf{X}_{c1} + \mathbf{D}_{c12}\mathbf{w} \\ \dfrac{\mathrm{d}}{\mathrm{d}t} i_{2t} = \mathbf{C}_{c2}\mathbf{B}_{c21}u_b + d_{c21}\dot{u}_b + (\mathbf{C}_{c2}\mathbf{B}_{c22} + \mathbf{D}_{c22}\mathbf{A}_1)\mathbf{X}_1 + \mathbf{D}_{c22}\mathbf{B}_1 \begin{bmatrix} i_{1t} \\ i_{2t} \end{bmatrix} \\ \qquad\qquad + \mathbf{C}_{c2}\mathbf{A}_{c2}\mathbf{X}_{c2} + \mathbf{D}_{c22}\mathbf{w} \end{cases} \tag{21}$$

Write out the two current state components in equation (21), as shown in equation (22).

$$\begin{cases} \dfrac{\mathrm{d}}{\mathrm{d}t} i_{1t} = \dfrac{1}{2}[(\mathbf{C}_{c1}\mathbf{B}_{c12} + \mathbf{D}_{c12}\mathbf{A}_1)\mathbf{X}_1 + (\mathbf{C}_{c2}\mathbf{B}_{c22} + \mathbf{D}_{c22}\mathbf{A}_1)\mathbf{X}_1] \\ \qquad + \dfrac{1}{2}\left[\mathbf{D}_{c12}\mathbf{B}_1 \begin{bmatrix} i_{1t} \\ i_{2t} \end{bmatrix} + \mathbf{D}_{c22}\mathbf{B}_1 \begin{bmatrix} i_{1t} \\ i_{2t} \end{bmatrix}\right] \\ \quad + \dfrac{1}{2}(\mathbf{C}_{c1}\mathbf{B}_{c11}u_a + \mathbf{C}_{c2}\mathbf{B}_{c21}u_b) + \dfrac{1}{2}(d_{c11}\dot{u}_a + d_{c21}\dot{u}_b) \\ \quad + \dfrac{1}{2}(\mathbf{C}_{c1}\mathbf{A}_{c1}\mathbf{X}_{c1} + \mathbf{C}_{c2}\mathbf{A}_{c2}\mathbf{X}_{c2}) + \dfrac{1}{2}(\mathbf{D}_{c12}\mathbf{w} + \mathbf{D}_{c22}\mathbf{w}) \\ \dfrac{\mathrm{d}}{\mathrm{d}t} i_{2t} = \dfrac{1}{2}[(\mathbf{C}_{c1}\mathbf{B}_{c12} + \mathbf{D}_{c12}\mathbf{A}_1)\mathbf{X}_1 + (\mathbf{C}_{c2}\mathbf{B}_{c22} + \mathbf{D}_{c22}\mathbf{A}_1)\mathbf{X}_1] \\ \qquad + \dfrac{1}{2}\left[\mathbf{D}_{c12}\mathbf{B}_1 \begin{bmatrix} i_{1t} \\ i_{2t} \end{bmatrix} + \mathbf{D}_{c22}\mathbf{B}_1 \begin{bmatrix} i_{1t} \\ i_{2t} \end{bmatrix}\right] \\ \quad + \dfrac{1}{2}(\mathbf{C}_{c1}\mathbf{B}_{c11}u_a + \mathbf{C}_{c2}\mathbf{B}_{c21}u_b) + \dfrac{1}{2}(d_{c11}\dot{u}_a + d_{c21}\dot{u}_b) \\ \quad + \dfrac{1}{2}(\mathbf{C}_{c1}\mathbf{A}_{c1}\mathbf{X}_{c1} + \mathbf{C}_{c2}\mathbf{A}_{c2}\mathbf{X}_{c2}) + \dfrac{1}{2}(\mathbf{D}_{c12}\mathbf{w} + \mathbf{D}_{c22}\mathbf{w}) \end{cases} \tag{22}$$

It can be seen from equation (22) that under the action of the current balance distribution matrix $\mathbf{T}$, even if the reference inputs of the two control channels are different, that is $u_a \neq u_b$ and $\dot{u}_a \neq \dot{u}_b$, the differentials of the two target currents, $\frac{\mathrm{d}}{\mathrm{d}t} i_{1t}$ and $\frac{\mathrm{d}}{\mathrm{d}t} i_{2t}$, are still equal.

In summary, the key to the control of the dual-redundancy system is to make the torques of the two motors equal. When performing torque balance control, it is actually to make the target currents equal. Through the above analysis, firstly, let the two controllers have the same structure and parameters, which can ensure that the two target currents are roughly the same. However, due to communication delays and asynchronous calculation rhythms, the reference inputs of the two control channels may be different. To solve this problem, a current balance distribution matrix is added to the original controllers, thus achieving balanced control of the torques of the two motors.

3.2 Multi-mode control of steering wheel system

According to the dual-redundancy control analysis, it can be known that the structure and parameters of two controllers are the same. Therefore, the following will only introduce the control of one motor in detail. The control method of the other one is the same.

In the analysis of the steering wheel system function, it can be known that under different vehicle driving conditions, the steering wheel system should work in different

modes. The two control mode estimation modules in Figure 2, 'Mode estimation 1' and "Mode estimation 2", are to determine which control mode the system should be in for the current driving condition.

The mode estimation module in Figure 2 is a state transition block, as shown in Figure 6.

Figure 6 Mode estimation module

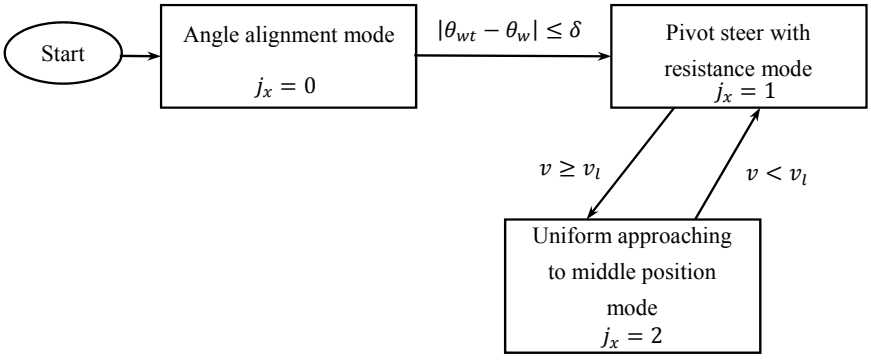

Figure 6 shows the transition process of the system control states. When the system is just powered on, it starts from the 'Start' state and automatically enters the 'Angle alignment mode' state, in which the control mode flag $j_x = 0$. This is because the steering wheel angle is not limited when the system is powered off and may turn to an unknown angle, while the steering gear angle does not change due to the restriction of the front wheels. Therefore, their angles may be different when the system power is just on. It is necessary to align their angles to prepare for the subsequent normal execution of the steering function.

When the difference between the actual angle and target angle is less than the threshold δ, that is, the state transition condition "$|\theta_{wt} - \theta_w| \leq \delta$" is satisfied, the system control state is transferred to the "Pivot steer with resistance mode".

After the angle alignment is completed, it is assumed that the vehicle has not started to move, so the driver should feel the resistance moment that hinders the steering wheel rotation and the steering wheel should remain still when it is not turned. So the control mode is transferred to "Pivot steer with resistance mode".

When the vehicle starts and the speed exceeds the threshold v_l, the steering wheel should imitate the mechanical steering system and has the tendency to actively return to the middle position. At the same time, the driver should feel the aligning torque during the rotation of the steering wheel. Therefore, the control mode becomes "Uniform approaching to middle position mode".

The above are the 3 different system working modes. The expanded view of the 'Multi-mode control' module in Figure 2 is shown in Figure 7.

Figure 7 Multi-mode control structure

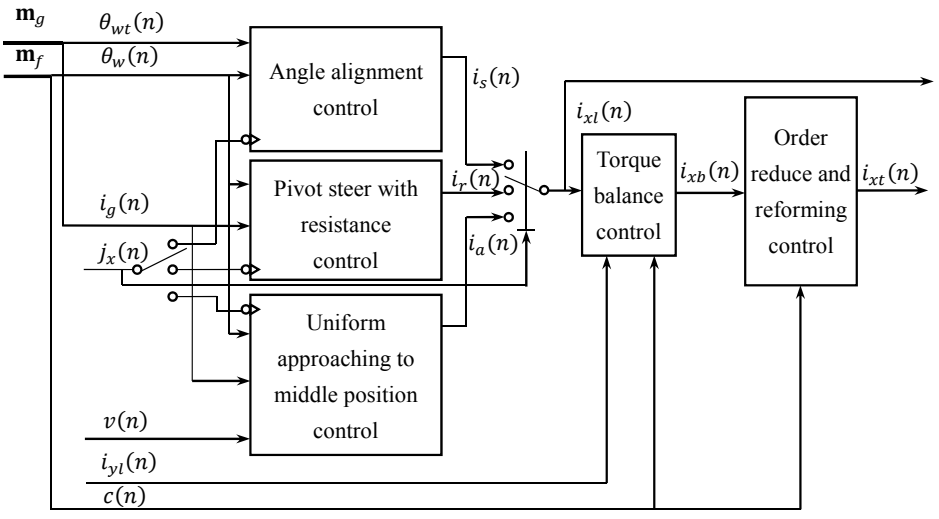

In Figure 7, all input and output signals are the inputs and outputs of the 'Multi-mode control' module in Figure 2. For specific description, please refer to the introduction below in Figure 2. It is important to note that the internal expansions of two 'Multi-mode control' modules are the same. The above figure illustrates any one of the two control modules. The j_x in the input signal represents the control mode flag signal of its own control channel, i_{yl} represents the unbalanced target current from another control channel and c represents another motor cut-off signal sent by the redundancy management module $\mathbf{F}$. The i_{xl} in the output signals represents the unbalanced target current sent by its own control channel to another channel and i_{xt} represents the target current sent to the motor of its own control channel.

Figure 7 contains three different control modes corresponding to the three control states in Figure 6. The j_x signal enables these three methods by a selection switch. Each time the j_x signal only makes one of the three control modules work, then j_x signal selects the output of the enabled module by controlling the selection switch behind the three modules. After obtaining the unbalanced target current i_{xl}, it passes through the 'Torque balance control' module and "Order reduce and reforming control" module. Finally the motor target current i_{xt} is obtained.

The above is the control architecture of multi-mode control. The following will introduce the three control modes.

3.2.1 Angle alignment mode control

Angle alignment control is the control that aligns the angle of the steering wheel to the corresponding angle of the steering gear when the system is just powered on. Therefore, this control is to approach the actual steering wheel angle to a certain target angle.

The control block diagram of angle alignment control is shown in Figure 8.

Figure 8 Angle alignment control

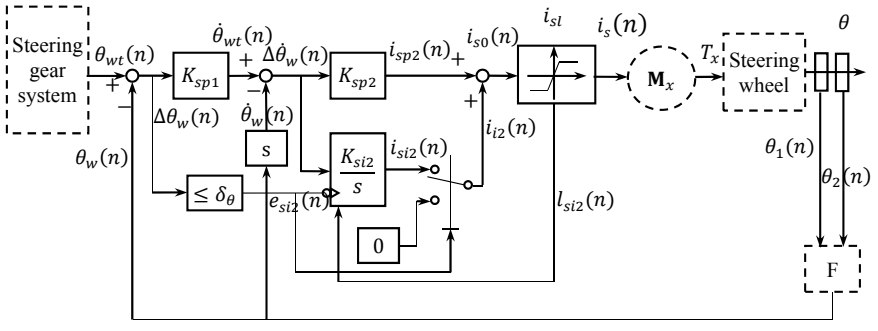

In Figure 8, the steering gear system sends the steering wheel target angle $\theta_{wt}(n)$. The target angle $\theta_{wt}(n)$ is compared with the actual steering wheel angle $\theta_w(n)$ to obtain the angle difference $\Delta\theta_w(n)$. After the calculation in angle-loop proportional controller "K_{sp1}", the target speed $\dot{\theta}_{wt}(n)$ is calculated. The calculation equations are shown in equation (23) and (24).

$$\Delta\theta_w(n) = \theta_{wt}(n) - \theta_w(n) \tag{23}$$

$$\dot{\theta}_{wt}(n) = K_{sp1}\Delta\theta_w(n) \tag{24}$$

The actual speed of the steering wheel $\dot{\theta}_w(n)$ is calculated by differentiating the actual steering wheel angle $\theta_w(n)$. After making a difference with the target speed $\dot{\theta}_{wt}(n)$, the proportional module target current $i_{sp2}(n)$ is obtained through the calculation of the speed-loop proportional control module "K_{sp2}". The calculation equations are shown in equations (25)–(27).

$$\dot{\theta}_w(n) = \frac{\theta_w(n) - \theta_w(n-1)}{\Delta t} \tag{25}$$

$$\Delta\dot{\theta}_w(n) = \dot{\theta}_{wt}(n) - \dot{\theta}_w(n) \tag{26}$$

$$i_{sp2}(n) = K_{sp2}\Delta\dot{\theta}_w(n) \tag{27}$$

$e_{si2}(n)$ is an enable signal, of which the calculation is shown in equation (28).

$$e_{si2}(n) = \begin{cases} 0 & (\Delta\theta_w(n) > \delta_\theta) \\ 1 & (\Delta\theta_w(n) \leq \delta_\theta) \end{cases} \tag{28}$$

$e_{si2}(n)$ is used to enable the integral module of the speed loop "$\frac{K_{si2}}{s}$". When the angle difference $\Delta\theta_w(n)$ is greater than the threshold δ_θ, the integral module "$\frac{K_{si2}}{s}$" does not work and the integral current $i_{i2}(n)$ is 0. When $\Delta\theta_w(n)$ is less than δ_θ, the signal $e_{si2}(n)$ enables the speed loop integral module "$\frac{K_{si2}}{s}$", which performs integral control

on the speed difference $\Delta\dot{\theta}_w(n)$. The integral current $i_{i2}(n)$ is equal to the output current $i_{si2}(n)$ of module "$\frac{K_{si2}}{s}$". The value of $i_{i2}(n)$ is shown in equation (29).

$$i_{i2}(n)=\begin{cases}0 & (e_{si2}(n)=0)\\ i_{si2}(n) & (e_{si2}(n)=1)\end{cases} \tag{29}$$

$i_{s0}(n)$ is the sum of $i_{sp2}(n)$ and $i_{i2}(n)$, as shown in equation (30).

$$i_{s0}(n)=i_{sp2}(n)+i_{i2}(n) \tag{30}$$

$l_{si2}(n)$ is the current saturation signal. When $i_{s0}(n)$ reaches the saturation value i_{sl}, the module outputs the limited current i_{sl} and changes $l_{si2}(n)$. Its value is shown in equation (31).

$$l_{si2}(n)=\begin{cases}0 & (i_{s0}(n)<i_{sl})\\ 1 & (i_{s0}(n)\geq i_{sl})\end{cases} \tag{31}$$

The algorithm of the speed loop integral module "$\frac{K_{si2}}{s}$" are shown in equation (32) and (33).

$$\Delta\dot{\theta}_{wi}(n)=\begin{cases}\Delta\dot{\theta}_w(n) & (l_{si2}(n)=0)\\ 0 & (l_{si2}(n)=1)\end{cases} \tag{32}$$

$$i_{si2}(n)=K_{si2}\sum_{m=1}^{n}\Delta\dot{\theta}_{wi}(m) \tag{33}$$

In equation (32), when $l_{si2}(n)=0$, the speed integral value $\Delta\dot{\theta}_{wi}(n)$ is equal to the speed difference $\Delta\dot{\theta}_w(n)$. The integral current $i_{si2}(n)$ is obtained through equation (33). When $l_{si2}(n)=1$, which means $i_{s0}(n)$ reaches the saturation value i_{sl}, the speed integral value $\Delta\dot{\theta}_{wi}(n)$ is equal to 0 and $i_{si2}(n)$ in equation (33) no longer increases, thus the integral oversaturation can be avoided.

The output of saturation limit module is motor target current $i_s(n)$. It is calculated as shown in equation (34).

$$i_s(n)=\operatorname{sgn}(i_{s0}(n))\min\{|i_{s0}(n)|,i_{sl}\} \tag{34}$$

The motor target current $i_s(n)$ is transmitted to the electric drive module $\mathbf{M}_x$ of this channel, which generates torque T_x on the steering wheel.

The angle alignment control method shown in Figure 8 only uses proportional control when the steering wheel angle and the target angle difference is relatively large, which avoids the oversaturation problem of integral control. After the angle difference becomes smaller, the proportional control almost loses its effect. At this time, integral control is introduced to eliminate the final static angle error. At the same time, the saturation limit module is used to prevent excessive output current.

3.2.2 Pivot steer with resistance mode control

After the steering wheel angle is aligned with the target angle, the system should perform the steering function normally. By default, the vehicle is at a standstill at this time. When the driver turns the steering wheel, the driver should feel the resistance torque opposite to the direction of rotation. In addition, the steering wheel should remain stationary after release. Therefore, the control in this mode is to reduce the steering wheel rotation speed to zero. At the same time, the resistance torque felt by the driver should be related to the steering resistance torque of the front wheels, so the current of steering gear motor needs to be introduced as the basis for the resistance torque value.

The control block diagram of pivot steer with resistance is shown in Figure 9.

Figure 9 Pivot steer with resistance control

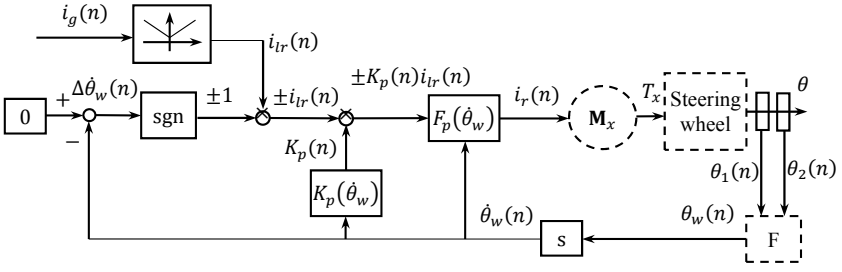

In Figure 9, module "0"is the target speed. The difference between the target speed and actual speed $\dot{\theta}_w(n)$, that is, the speed difference $\Delta\dot{\theta}_w(n)$ is obtained. Then the direction of the resistance current is calculated by the symbol function module " sgn ", which is $+1$ or -1.

The steering gear motor current $i_g(n)$ passes through the linear value module to calculate the resistance current value $i_{lr}(n)$. The calculation of this module is shown in equation (35).

$$i_{lr}(n) = K_{lr}\left|i_g(n)\right| + B_{lr} \tag{35}$$

The resistance current value $i_{lr}(n)$ has a linear relationship with the absolute value of steering gear motor current $i_g(n)$. The proportional coefficient K_{lr} and intercept term B_{lr} can be adjusted according to driver needs.

The resistance current value $i_{lr}(n)$ is multiplied by the current direction, which is $+1$ or -1, to obtain the resistance current with direction $\pm i_{lr}(n)$.

The " $K_p(\dot{\theta}_w)$ " module is a current suppression module. Its calculation formula is shown in equation (36).

$$K_p(n) = \begin{cases} 0 & \left|\dot{\theta}_w(n)\right| \le \delta_\omega \\ 1 & \left|\dot{\theta}_w(n)\right| > \delta_\omega \end{cases} \tag{36}$$

When the absolute value of the steering wheel rotational speed $\left|\dot{\theta}_w(n)\right|$ is less than the threshold δ_ω, it is considered that the steering wheel is not rotating at this time, then no torque should be generated on the steering wheel. When $\left|\dot{\theta}_w(n)\right|$ exceeds the threshold δ_ω, the steering wheel is considered to be turned by the driver, then the resistance torque is applied. This module is to prevent the wrong application of torque caused by the small steering wheel angle vibration.

$K_p(n)$ is multiplied by $\pm i_{lr}(n)$ and then calculated by the conditional filter module "$F_p\left(\dot{\theta}_w\right)$". Its equation is shown in equation (37) and (38).

$$f_p(n)=\begin{cases}1 & \left|\dot{\theta}_w(n)\right|\le\delta_\omega\\ K_f & \left|\dot{\theta}_w(n)\right|>\delta_\omega\end{cases} \tag{37}$$

$$i_r(n)=i_r(n-1)+f_p(n)\left[\pm K_p(n)i_{lr}(n)-i_r(n-1)\right] \tag{38}$$

According to equation (37), when the absolute rotation speed $\left|\dot{\theta}_w(n)\right|$ is less than the threshold δ_ω, the filter coefficient $f_p(n)$ is 1. Then the output current $i_r(n)$ is equal to $\pm K_p(n)i_{lr}(n)$. According to equation (36), since $K_p(n)$ is 0 in this condition, the output current value $i_r(n)$ is 0 and no torque is generated on the steering wheel. When $\left|\dot{\theta}_w(n)\right|$ is greater than the threshold δ_ω, the filter coefficient $f_p(n)$ is K_f, which is less than 1. At this time, according to equation (38), the module has a filtering effect on the input current $\pm K_p(n)i_{lr}(n)$. The output current $i_r(n)$ gradually transitions from the current value to the input current value $\pm K_p(n)i_{lr}(n)$.

The conditional filtering module is used, so that the resistance torque felt by the driver gradually increases within a certain period of time when the steering wheel starts to turn, rather than a step resistance torque. The steering wheel speed decreases after release. When it is lower than the threshold, the resistance torque should be cancelled immediately to avoid the torque still being applied for the filtering hysteresis effect, which may cause the steering wheel to oscillate.

In the pivot steer with resistance control, when the vehicle speed is less than the threshold, a resistance torque opposite to the rotation direction is generated on the steering wheel, which can reflect the change of the steering resistance torque of the front wheels. At the same time, when the steering wheel starts to rotate, the resistance torque is gradually established and cancelled when its speed is reduced, so as to avoid the angle oscillation of the steering wheel.

3.2.3 Uniform approaching to middle position control during running

When the vehicle speed exceeds the threshold v_l, according to the state flow in Figure 6, the steering wheel control enters "Uniform approaching to middle position" mode. In this control mode, the steering wheel always has a tendency to move to the middle position, which means the target angle is 0 degree. After the driver holds the steering wheel, the steering torque should be able to reflect the changes in the steering resistance torque of the front wheels. After release, the steering wheel should uniformly converge to 0 degree under the control of the motor.

The uniform approaching to middle position control block diagram is shown in Figure 10.

Figure 10 Uniform approaching to middle position control

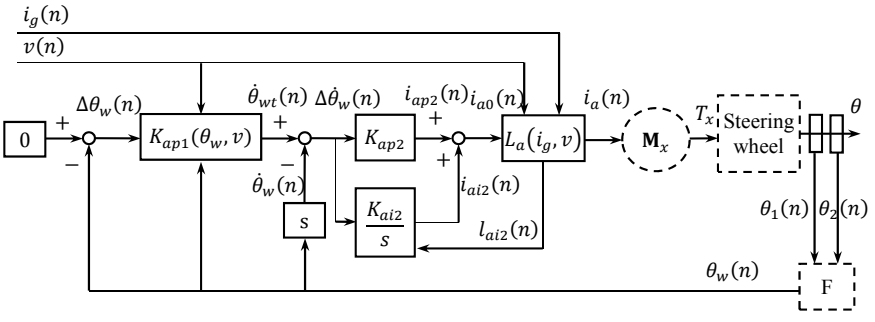

In Figure 10, module "0" is the steering wheel target angle. After making the difference between it and the feedback angle $\theta_w(n)$, the angle difference $\Delta\theta_w(n)$ is obtained. The module "$K_{ap1}(\theta_w, v)$" is a proportional control module of angle loop with variable proportional coefficient. The calculations in this module are shown in equation (39) and (40).

$$K_{ap1}(n) = K_{ap1}(\theta_w(n), v(n)) \tag{39}$$

$$\dot{\theta}_{wt}(n) = K_{ap1}(n)\Delta\theta_w(n) \tag{40}$$

In equation (39), the proportional coefficient $K_{ap1}(n)$ is a function of steering wheel angle $\theta_w(n)$ and vehicle speed $v(n)$. This coefficient is multiplied by the angle difference $\Delta\theta_w(n)$ to obtain the target speed of the steering wheel $\dot{\theta}_{wt}(n)$ in equation (40).

The coefficient $K_{ap1}(n)$ is designed as a variable function in order to design different steering wheel align speeds according to vehicle speeds and angles to meet the driver's requirements.

Differentiate $\theta_w(n)$ to obtain the steering wheel speed $\dot{\theta}_w(n)$. Make the difference between the target speed $\dot{\theta}_{wt}(n)$ and $\dot{\theta}_w(n)$ to obtain the speed difference $\Delta\dot{\theta}_w(n)$. Module "K_{ap2}" is the proportional controller of speed loop. Its calculation is shown in equation (41).

$$i_{ap2}(n) = K_{ap2}\Delta\dot{\theta}_w(n) \tag{41}$$

The integral module "$\frac{K_{ai2}}{s}$" of speed loop is an integral controller enabled by an anti-saturation signal l_{ai2}. It is calculated as shown in equation (42) and (43).

$$\Delta\dot{\theta}_{wa}(n) = \begin{cases} \Delta\dot{\theta}_w(n) & (l_{ai2}(n) = 0) \\ 0 & (l_{si2}(n) = 1) \end{cases} \tag{42}$$

$$i_{ai2}(n) = K_{ai2}\sum_{m=1}^{n}\Delta\dot{\theta}_{wa}(m) \tag{43}$$

The calculation logic of equations (42) and (43) are similar to that of equations (32) and (33). When the current is not saturated, the integration proceeds normally. If the current is saturated, the speed difference used for integration $\Delta\dot{\theta}_{wa}(n)$ is 0 and the integral value does not increase.

After summing the output current of the proportional controller $i_{ap2}(n)$ and the integral controller $i_{ai2}(n)$ in speed-loop control, the current to be limited $i_{a0}(n)$ is obtained, as shown in equation (44).

$$i_{a0}(n) = i_{ap2}(n) + i_{ai2}(n) \tag{44}$$

The module "$L_a(i_g, v)$" is a current limit module, which is also a module that enables the driver to feel the change in the steering resistance torque of the front wheels. It is calculated as shown in equations (45)–(47).

$$i_{la}(n) = K_{la}(v(n))\left|i_g(n)\right| + B_{la}(v(n)) \tag{45}$$

$$i_a(n) = \operatorname{sgn}(i_{a0}(n))\min\left\{\left|i_{a0}(n)\right|, i_{la}(n)\right\} \tag{46}$$

$$l_{ai2}(n) = \begin{cases} 0 & \left(\left|i_{a0}(n)\right| < i_{la}(n)\right) \\ 1 & \left(\left|i_{a0}(n)\right| \geq i_{la}(n)\right) \end{cases} \tag{47}$$

In equation (45), the motor current limit $i_{la}(n)$ is calculated according to the absolute value of the steering gear motor current $\left|i_g(n)\right|$. This limit $i_{la}(n)$ has a linear relationship with $\left|i_g(n)\right|$, so that the change in the limit can reflect the change in the steering resistance torque of front wheels. The proportional coefficient $K_{la}(v(n))$ and intercept terms $B_{la}(v(n))$ are functions of vehicle speed $v(n)$. This is to adjust the amount of torque that the driver feels according to different vehicle speeds.

Equation (46) limits $i_{a0}(n)$ within the current limit $i_{la}(n)$ as the motor target current $i_a(n)$. Equation (47) compares $i_{a0}(n)$ with $i_{la}(n)$. When $i_{a0}(n)$ reaches $i_{la}(n)$, the anti-saturation signal $l_{ai2}(n)$ is changed to prevent the integral controller from over-saturating.

In summary, after the vehicle has a certain speed, the control method takes 0 degree as the target angle, which means the steering wheel has a tendency to align to the middle position. When the driver holds the steering wheel, it cannot reach the target speed and the integral controller continuously increases the current. When it reaches the current limit that is linear with the steering gear motor current, the current does not increase, so that the driver feels the changes in the steering resistance torque of the front wheels. The torque can also be adjusted with the vehicle speed to reach the driver's satisfaction.

When the driver releases the steering wheel, this control method automatically controls the steering wheel to 0 degree angle, so as to realise the free return of the steering wheel.

3.3 Torque balance control

After calculating the output currents of three different control modes, the selector switch selects the output signal of the enabled module according to the control mode flag j_x to obtain the current to be balanced i_{xl} as shown in Figure 7. The current i_{xl} is calculated by the torque balance control module to obtain the balanced current i_{xb}.

According to the analysis in section 3.1, in order to balance the output target currents, two points need to be ensured: First, the controller structure and parameters of two controllers are the same. Second, add a current balance distribution matrix $\mathbf{T}$ to the outputs of the two controllers. The first point has been described in Section 3.2, that is, the two controllers are internally the same. To satisfy the second point, the "Torque balance control" module in Figure 7 is proposed.

The calculation of the "Torque balance control" in Figure 7 is shown in the following equation (48).

$$i_{xb}(n)=\begin{cases}\dfrac{1}{2}\left(i_{xl}(n)+i_{yl}(n)\right) & \left(c(n)=0\right)\\ i_{xl}(n) & \left(c(n)=1\right)\end{cases} \tag{48}$$

In equation (48), when $c(n)=0$, there is no fault in the system. According to the calculation of matrix $\mathbf{T}$, the output current should be the average value of the inputs, so the balance current $i_{xb}(n)$ should be the average value of the outputs of two control channels $i_{xl}(n)$ and $i_{yl}(n)$. When $c(n)=1$, the redundancy management $\mathbf{F}$ in Figure 2 identifies a fault in the system and cuts off the power of the other channel motor. In this case, to isolate the information of another channel, the output only takes the result $i_{xl}(n)$, $i_{yl}(n)$ is no longer used for calculation. In order to make the currents before and after the fault basically the same, the averaging calculation is removed, only the current $i_{xl}(n)$ of the channel controller is used as the output $i_{xb}(n)$ of the channel.

3.4 Order-reduce and reforming control

When a order-reduce fault occurs in the system, the redundancy management module $\mathbf{F}$ recognises the fault and cuts off the power of the corresponding motor. Only the other motor is used to control the steering wheel. In this case, the driver's steering torque before and after the failure should be maintained basically unchanged, so as to ensure driving safety as much as possible.

In the case of an order-reduce fault, one dimension in the input $\mathbf{u}_1$ in Figure 5 becomes 0. In order to ensure that the torque on the mechatronics system remains unchanged, equation (6) is investigated. Assuming that the current in the second dimension of $\mathbf{u}_1$ becomes 0 after the fault and the current in the first dimension becomes $i_{1t}^{'}$, then equation (6) becomes the following equation.

$$\begin{cases} \dot{\mathbf{X}}_1 = \begin{bmatrix} 0 & 1 \\ 0 & -\dfrac{B}{J} \end{bmatrix} \mathbf{X}_1 + \begin{bmatrix} 0 & 0 \\ \dfrac{K_T\varphi}{J} & \dfrac{K_T\varphi}{J} \end{bmatrix} \begin{bmatrix} i_{1t}^{'} \\ 0 \end{bmatrix} + \begin{bmatrix} 0 \\ \dfrac{T_h - T_f}{J} \end{bmatrix} \\ y = \begin{bmatrix} 1 & 0 \end{bmatrix} \mathbf{X}_1 \end{cases} \tag{49}$$

In order to ensure that the track of states $\mathbf{X}_1$ in equations (6) and (49) are the same, it is only necessary to ensure that the inputs of the systems are the same, as shown in equation (50).

$$\begin{bmatrix} 0 & 0 \\ \dfrac{K_T\varphi}{J} & \dfrac{K_T\varphi}{J} \end{bmatrix} \begin{bmatrix} i_{1t}^{'} \\ 0 \end{bmatrix} = \begin{bmatrix} 0 & 0 \\ \dfrac{K_T\varphi}{J} & \dfrac{K_T\varphi}{J} \end{bmatrix} \begin{bmatrix} i_{1t} \\ i_{2t} \end{bmatrix} \tag{50}$$

Therefore, the current after the fault $i_{1t}^{'}$ should be the sum of the current before the fault, as shown in equation (51).

$$i_{1t}^{'} = i_{1t} + i_{2t} \tag{51}$$

However, since the information in the second control channel is no longer credible after the fault, the current in channel 1 is expanded by a certain multiple as the approximation of the sum of the two, as shown in equation (52).

$$i_{1t}^{'} = K_r i_{1t} \tag{52}$$

In equation (52), K_r is the current gain coefficient. The specific coefficient needs to be determined according to the driver's inability to experience significant torque changes before and after the fault in vehicle test.

Therefore, the calculation of the "Order-reduced and reforming control" in Figure 7 is as shown in equation (53).

$$i_{xt}(n) = \begin{cases} i_{xb}(n) & (c(n) = 0) \\ K_r i_{xb}(n) & (c(n) = 1) \end{cases} \tag{53}$$

In equation (53), when the system has no fault, $c(n) = 0$, the output current $i_{xt}(n)$ is the balanced current $i_{xb}(n)$. When a order-reduced fault occurs in another channel, $c(n) = 1$. At this time, the balanced current of this channel $i_{xb}(n)$ is multiplied by a certain gain K_r as the output $i_{xt}(n)$ to ensure that the torque felt by the driver before and after the fault is basically unchanged.

Through the order-reduce and reforming control, it is ensured that when the power of one motor in the system is cut off, the other motor will continue to work. The driver will feel basically the same steering torque before and after the failure, thus ensuring the high safety and reliability of system functions.

4 Experiments of vehicle test and analysis

In order to verify the dual-redundancy multi-mode control method of the high safety reliability steering wheel system proposed above, a prototype is designed and manufactured according to the structure diagram shown in Figure 1. The prototype is installed in a real vehicle, building a real vehicle test platform.

Through various experiments on this platform, the proposed angle alignment control, pivot steer with resistance control, uniform approaching to middle position control, torque balance control and order-reduce and reforming control method are verified.

The following will introduce the test platform, the results and the analysis of each test.

4.1 Vehicle test platform with high safety reliability steering wheel system

According to the electromechanical structure of the steering wheel system shown in Figure 1, a prototype is designed and manufactured, as shown in Figure 11.

Figure 11 Prototype of the steering wheel system electromechanical structure (see online version for colours)

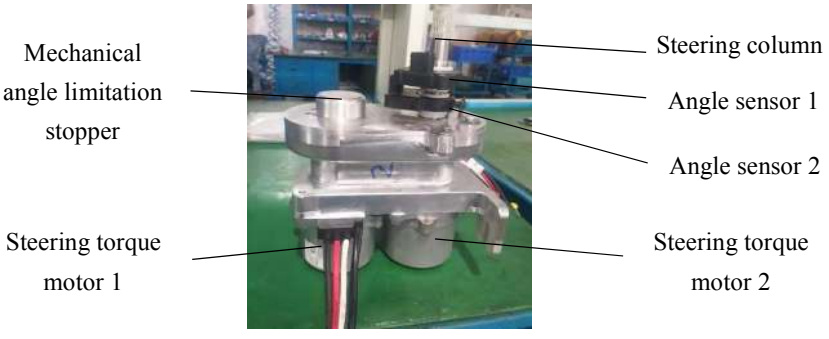

As shown in Figure 11, each part of it corresponds to the structure diagram in Figure 1. The steering wheel is sleeved on the steering column through splines, so as to realise the mechanical connection with the structure. It should be pointed out that the above structure does not include the electronic control motor drivers and the three controllers in the system.

According to the SBW structure in Figure 1, in order to cooperate with the steering wheel system, a steering gear system is designed and manufactured as well. Its electromechanical structure prototype is shown in Figure 12.

Figure 12 shows the structure of the steering gear, which contains two steering motors jointly pushing a rack to move. The rack drives the steering actuator to achieve the deflection of the front wheels.

Replace the original mechanical steering system of the test vehicle with the SBW shown in Figures 11 and 12. The installation picture of the steering wheel system is shown Figure 13.

Figure 12 Steering gear system electromechanical structure prototype (see online version for colours)

Figure 13 The installation picture of the steering wheel system (see online version for colours)

Figure 13 shows the steering wheel system with high safety and reliability installed on the test vehicle. In the figure, the electronic control driver of one of the motors can be observed.

The steering wheel system with high safety reliability vehicle test platform is shown in Figure 14.

In Figure 14, the steering wheel system is in front of the driver and the three controllers of the system are on the right under the windshield. The data acquisition equipment is connected to the network of the system. The data acquisition and display are operated through the PC.

The vehicle test is carried out on a medium-sized SUV, as shown in Figure 15.

Figure 14 Steering wheel system with high safety reliability vehicle test platform (see online version for colours)

Figure 15 Test vehicle picture (see online version for colours)

On the vehicle test platform, the dual-redundancy multi-mode control method proposed in Section 3 is verified. The test results and analysis of each method are introduced below.

4.2 Angle alignment control test

Firstly, the experimental verification of the angle alignment control method is carried out.

Before the angle alignment control test, the vehicle is powered off. The steering wheel stops at a position that does not correspond to the steering gear angle. After the system is powered on, the angle alignment control method controls the steering wheel to rotate to the target angle. The steering wheel angle curves measured by two angle sensors are shown in Figure 16.

Figure 16 Steering wheel target angle and angle signals of two angle sensors

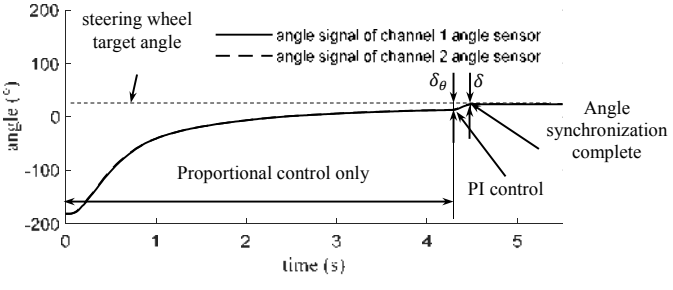

The solid line and the dashed line in Figure 16 are the steering wheel angles measured by the two angle sensors. When the system is just powered on, that is, when $t = 0s$, the steering wheel is at about $-182°$. Then the steering wheel moves closer to the target angle. Between $t = 0s$ and $t = 4.3s$, a proportional control method is used. The steering wheel speed gradually slows down as the angle is approaching the target. After $t = 4.3s$, according to the control block diagram in Figure 8, since the angle difference is less than the threshold δ_θ, an integral control module is added to the speed loop. At this time, the steering wheel angle accelerates and continues to approach the target angle until the angle difference is less than the threshold δ in Figure 6.

The target current curves of two channel motors are shown in Figure 17.

Figure 17 Target currents of two motors

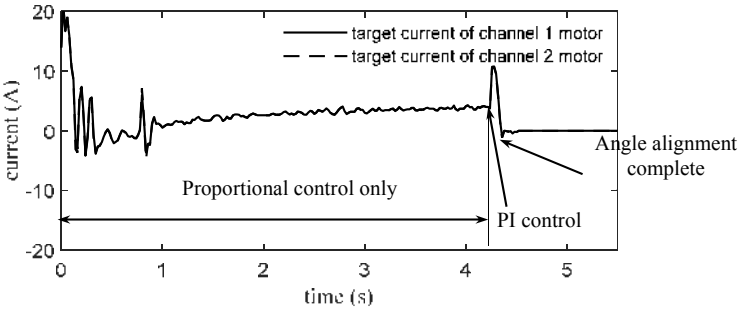

The solid and dashed lines in Figure 17 are the target current curves of the two motors. At the initial moment, the angle difference is large, so relatively large target currents are generated to quickly push the steering wheel to rotate. As the rotation speed increases, the currents oscillate to control the rotation speed. Between $t = 1s$ and $t = 4.3s$, the currents gradually stabilise. This is due to the slow change of the angle difference, resulting in the target speed being basically constant. Meanwhile, the actual steering wheel speed tends to 0, so nearly constant target currents are generated under proportional control. After $t = 4.3s$, due to the integral control, the currents rise rapidly, further pushing the steering wheel to move. After completing the angle alignment, the target currents return to 0 A and the steering wheel stays still.

The actual current curves of two motors are shown in Figure 18.

Figure 18 Actual currents of two motors

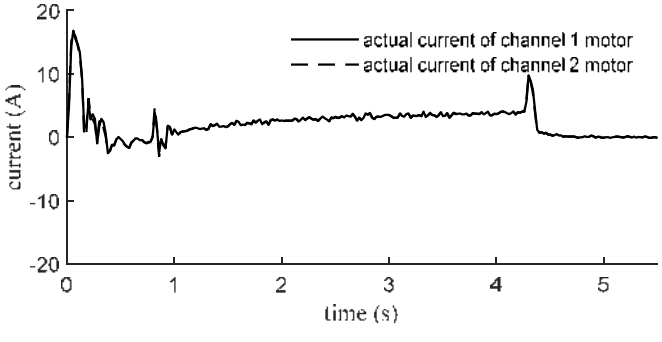

In Figure 18, the actual currents of two motors are basically the same as the target currents in Figure 17, indicating that the motors generate corresponding currents to drive the steering wheel to rotate.

The curves of the control mode flags are shown in Figure 19.

In Figure 19, when the angle alignment is completed, the flags jump to 1, which means the system enters normal working mode.

The above vehicle test of angle alignment shows that when the system is just powered on, this control method can align the steering wheel angle with the corresponding angle

of the steering gear, so that the system enters the normal control mode and prepares for the subsequent steering operation.

Figure 19 Control mode flags of two channels

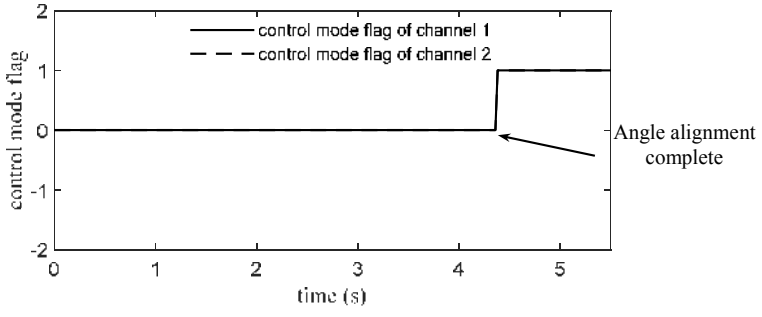

4.3 Pivot steer with resistance control test

After the steering wheel angle and the steering gear angle are aligned, the system enters the control mode of pivot steer with resistance. During the test, the vehicle remains stationary, the driver turns the steering wheel and then releases, and then continues to turn the steering wheel. The two processes alternate.

The steering wheel angle and motor target current curves in the test are shown in Figure 20.

Figure 20 Steering wheel angles and target currents of two channels in pivot steer test

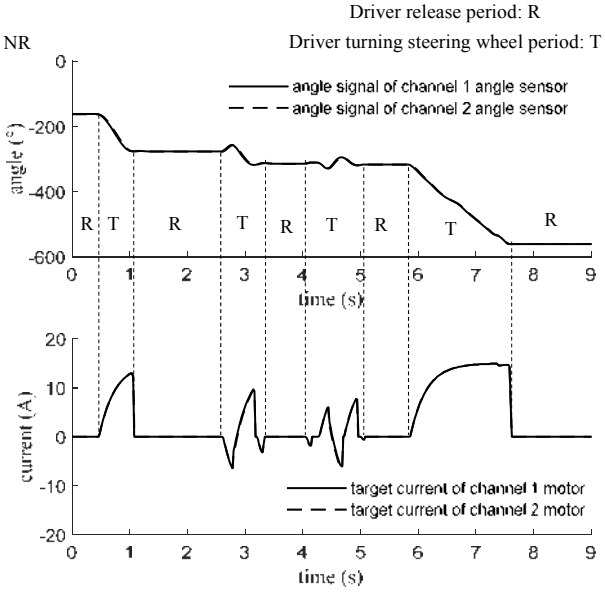

In Figure 20, the upper picture shows the steering wheel angles measured by two angle sensors. In the figure, the time period marked ‘R’ is the driver release phase and ‘T’ is the

driver turning phase. The lower figure shows the target current curves of two motors. The comparison of the upper and lower pictures shows that when the driver turns the steering wheel, the two motors simultaneously generate currents in the opposite direction to the rotation speed, which means the driver feels the resistance during turning the steering wheel. When the driver releases the hands, the target currents of the two motors are zero and the steering wheel can remain stationary. The above process conforms to the driver's steering operation habit when the vehicle is stationary.

In order to explain in detail the resistance control in the process of turning the steering wheel, expand the 5.5 s to 8 s in Figure 20 to obtain Figure 21.

Figure 21 Partial expanded view of steering wheel angles, speeds and target currents of two channels in pivot steer test

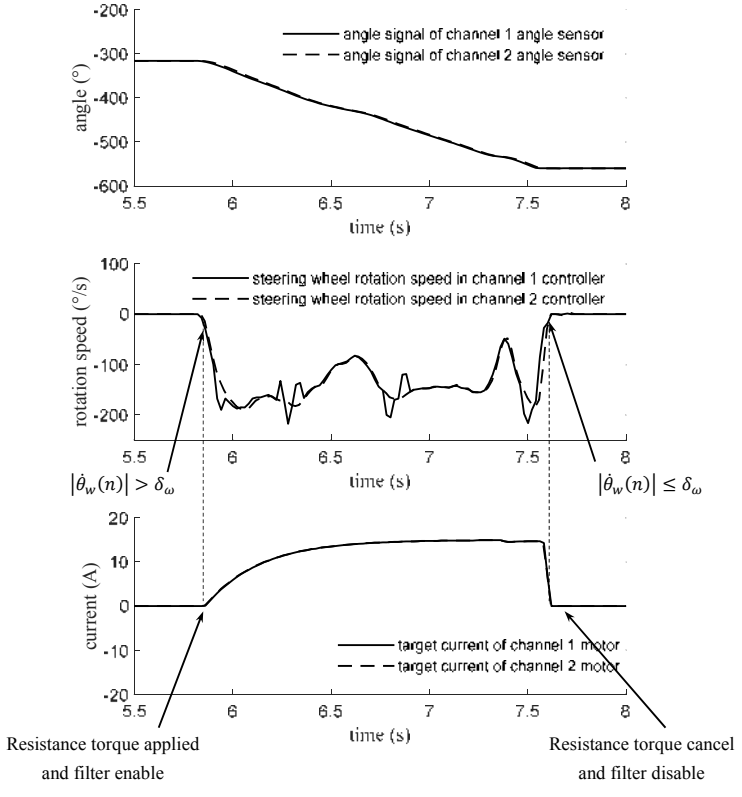

The first picture in Figure 21 shows the steering wheel angles measured by two angle sensors. The middle graph are the differential of the two curves in the first graph, which are the speed curves. It can be seen from the figure that the two rotational speed curves are roughly the same, but due to communication delays and asynchronous calculations, there are some differences in the speed curves. The third picture shows the target current curves of the two motors.

Putting the three pictures together for comparison, the control process can be analysed in detail. When the driver starts to turn the steering wheel, the speed exceeds the threshold, that is $\left|\dot{\theta}_w(n)\right| > \delta_\omega$, $K_p(n)$ is equal to 1 in equation (36), thus resistance on the steering wheel is applied. The target current is controlled by the filtering algorithm in

Equation (38) and gradually rises without a step. After the driver completes the steering, the speed gradually falls back to within the threshold, that is, when $\left|\dot{\theta}_w(n)\right| \le \delta_\omega$, $K_p(n) = 0$ in equation (36), the resistance torque is cancelled. According to equations (37) and (38), the filtering algorithm loses its effect. In the third figure, the current curves immediately drop to 0 and the steering wheel can remain stationary. If the filtering algorithm is not cancelled immediately after the end of the steering, the currents will drop slowly and the steering wheel will turn in the reverse direction, which is an undesirable result of the driver.

The pivot steer with resistance test results show that the control realises that when the vehicle is stationary, the resistance torque is established relatively smoothly when the driver starts to turn the steering wheel and quickly cancelled after the turning to ensure that the steering wheel can remain still. The steering control in line with the driver's operation habits is realised when the vehicle is stationary.

4.4 Uniform approaching to middle position test

When the vehicle is in motion, the steering wheel should always have a tendency to return to the middle position. When the driver releases the steering wheel, it should be able to return to the middle position and then remain still.

During the vehicle test, the vehicle keeps running and the vehicle speed curve is shown in Figure 22.

Figure 22 Vehicle speed in uniform approaching to middle position test

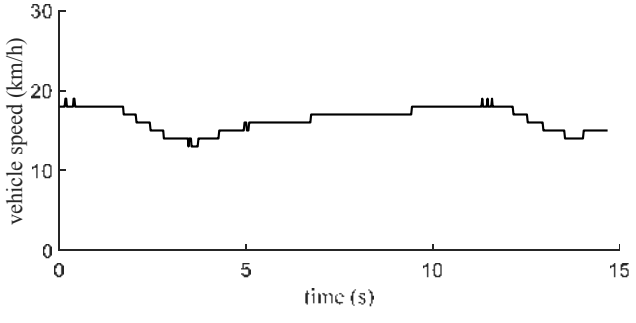

In Figure 22, the vehicle speed remains between 13 km/h and 19 km/h.

The steering wheel angle and speed curves are shown in Figure 23.

The upper picture in Figure 23 shows the steering wheel angle curves and the lower picture is the steering wheel target speed and actual speed curves. In the upper picture, the driver turns the steering wheel from the middle position to about 360° and then releases it. The steering wheel starts to return to the middle position. It returns to within 0.5° in 1.7 s. Next, the driver turns the steering wheel in the reverse direction and repeats the above process. The steering wheel returns from about –360° to within –3.9° in 2.1 s. The steering wheel angle is smooth during the process of free return, no vibration or overshoot in the process. The lower picture shows the speed tracking curves. When the driver turns the steering wheel, its speed is controlled by the driver and the target speeds are not tracked. After the driver releases the hands, the actual speed curves rise rapidly from 0, indicating that the steering wheel starts to rotate. After the actual speeds track the

targets, they gradually decrease with the targets until the steering wheel returns to the middle position.

Figure 23 Steering wheel angles and speeds of two channels in uniform approaching to middle position test

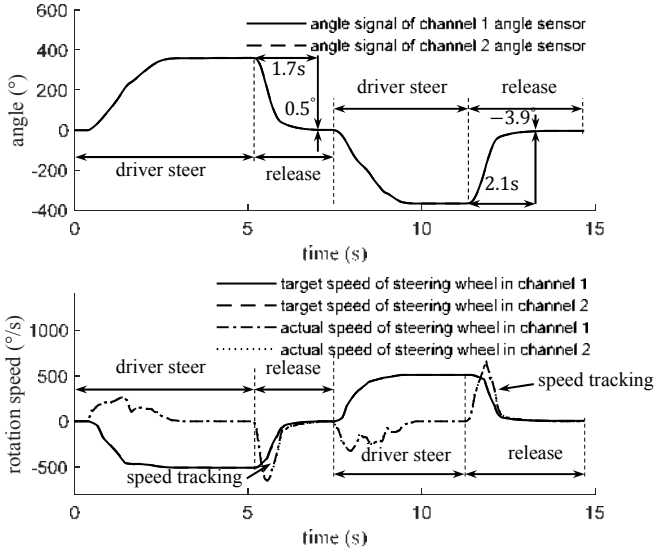

The current curves of two motors and the steering gear motor during the test are shown in Figure 24.

Figure 24 Currents of two channel motors and steering gear motor in uniform approaching to middle position test

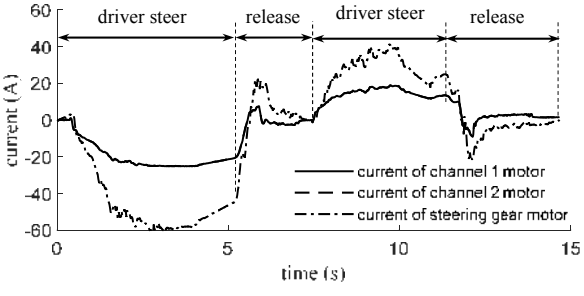

In Figure 24, the solid line and dash line are the current curves of the two channel motors, the dot dash line is the current of steering gear motor. In the two stages of driver steering, the currents of the two channel motors are linearly related to the steering gear motor current. This relationship becomes insignificant when the driver releases his hands. This is due to the $L_a\left(i_g, v\right)$ module in Figure 10 being effective in the previous stage but not working in the latter. This shows that when the driver controls the steering wheel, the torque that varies with the steering resistance torque can be felt, which is a relatively realistic road feel. After releasing the steering wheel, controlling the steering wheel to

return to the middle position becomes a priority, so the linear relationship of current is broken by the steering wheel angle control.

The vehicle test proves that the uniform approaching to middle position control method can make the driver feel the road feel linearly changing with the steering resistance torque when turning the steering wheel. At the same time, the method actively controls the steering wheel to return to the middle position after release. The free return process is smooth, without oscillation or overshoot.

4.5 Torque balance control test

In the torque balance control vehicle test, the vehicle speed is maintained at about 9 km/h and the driver turns the steering wheel. The unbalanced, the balanced target currents as well as the actual currents of the two motors are examined to prove its effectiveness.

The target steering gear angle calculated from the steering wheel angle θ_w and the actual steering gear angle curves are shown in Figure 25.

Figure 25 Target angle and actual angle of steering gear system in torque balance control test

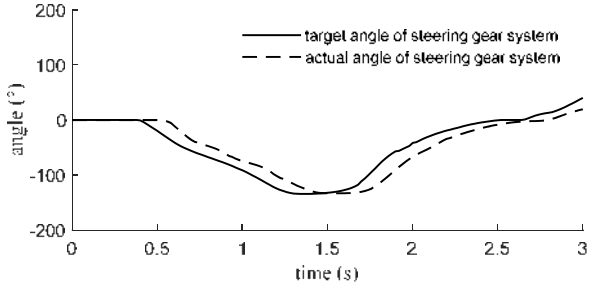

The solid line in Figure 25 is the target angle of steering gear calculated from the steering wheel angle θ_w. The dashed line is the actual angle of steering gear. The dashed line tracks the solid line well, indicating that the vehicle is turning normally under the control of the driver in the test.

The reference inputs of the two control channels, namely the fused steering wheel angles, and the rotation speeds of steering wheel obtained through angle differentiation are shown in Figure 26.

In the upper figure of Figure 26, there are the actual angles of the steering wheel. The two signals are equivalent to u_a and u_b in Figure 5. Theoretically, the two signals should be the same, but in fact they are different due to communication delays, asynchronous operating cycles, etc. The difference is not obvious in the upper figure, but it can be better illustrated in the lower figure.

Shown in the lower figure are the steering wheel rotation speed curves. The two speed curves are roughly the same, but in the circled part, the difference between the two curves can be clearly observed. In other words, the differential of the reference input of the two controllers is different, which means there is a significant difference between $\dot{u}_a$ and $\dot{u}_b$ in equation (21).

The difference of the reference inputs will cause the unbalanced target currents of the two motors to be significantly different, as shown in Figure 27.

Figure 26 Steering wheel angle and rotation speed messages in two channels

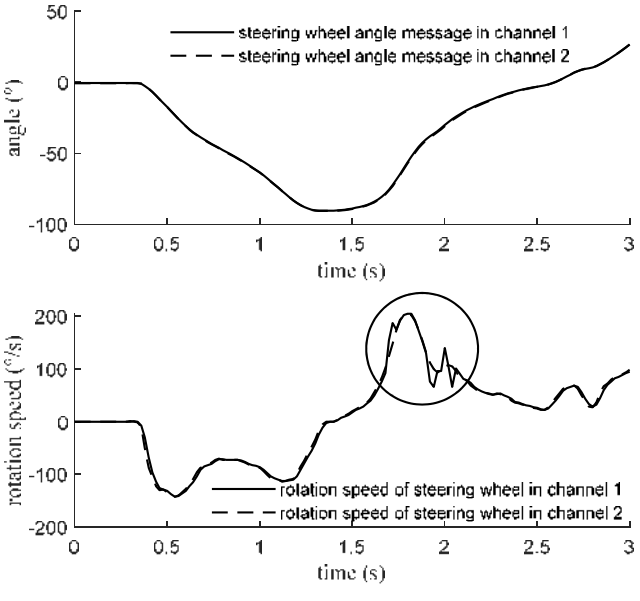

Figure 27 Unbalanced target currents of two motors

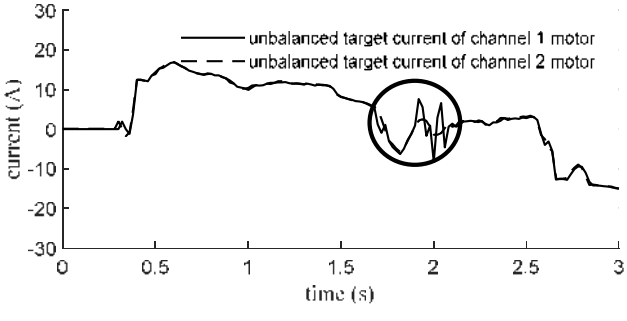

The solid line and the dashed line in Figure 27 are the unbalanced target currents of the channel 1 and channel 2 motors. The two currents are roughly the same, but there is a clear difference between the two in the circled position. The maximum difference is 7.6 A. The time the current difference occurs is the same as the time when the rotational speeds in Figure 26 is obviously different, which indicates that the difference in rotational speeds causes the difference in currents.

In order to solve the problem, a current balance distribution module **T** is added to the control structure. The balanced target currents and actual currents are shown in Figure 28.

The upper picture in Figure 28 are the target currents of the two motors after balance. The two curves are basically the same, especially where there are obvious differences between the unbalanced target currents in Figure 27, indicating that the torque balance control has worked. The lower figure shows the actual currents of the two motors,

which are basically the same under the same target currents, indicating that the two motor torques are basically the same. The torque balance control method proposed is verified.

Figure 28 Balanced target currents and actual currents

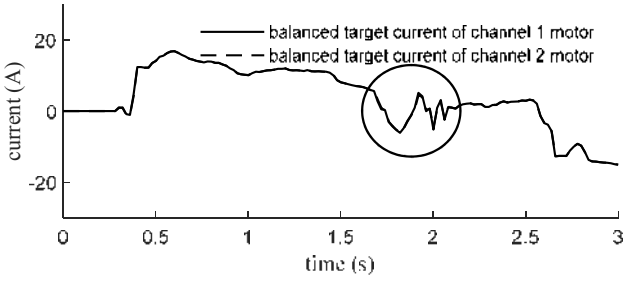

4.6 Order-reduce and reforming control test

During the operation of the system, if an order-reduce fault occurs, the system will cut off the power supply of the corresponding motor and the other one continues to work.

During the vehicle test, the driver turns the steering wheel. A fault is injected to channel 1 controller, which is cutting its power supply, to test the method effectiveness. The vehicle speed curve is shown in Figure 29.

Figure 29 Vehicle speed in order-reduce and reforming test

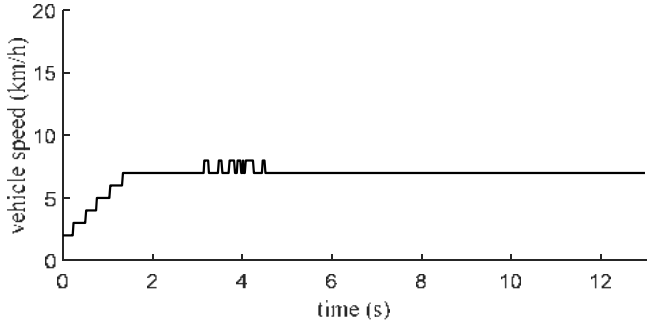

The speed of the vehicle gradually increases and remains at approximately 7 km/h.

The steering wheel angle signals in the two channel controllers collected on the dual-redundancy network are shown in Figure 30.

The upper and lower pictures in Figure 30 are the angle signals of channel 1 and channel 2 controller. The signal of channel 1 controller disappears at 6.4 s, indicating that the controller is malfunctioning and the channel 2 controller is working normally.

In the case of a failure of channel 1 controller, the dual-redundancy management module **F** in Figure 2 diagnoses the failure and cuts off the motor power supply of the

failed channel. At the same time, the cut information is sent to channel 2 controller, so that the channel 2 control can be reformed.

Figure 30 Angle signals from two channel controllers in order-reduce and reforming test

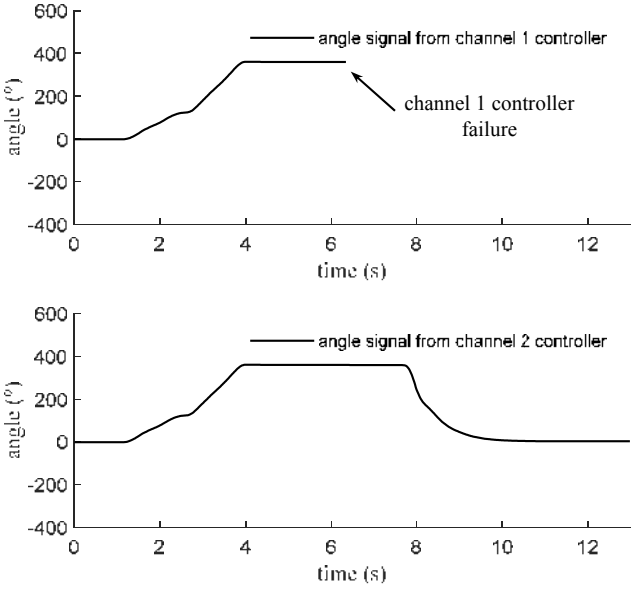

The power supply cutting signals sent to two channels are shown in Figure 31.

Figure 31 Cutting signals of two channel motor powers in order-reduce and reforming test

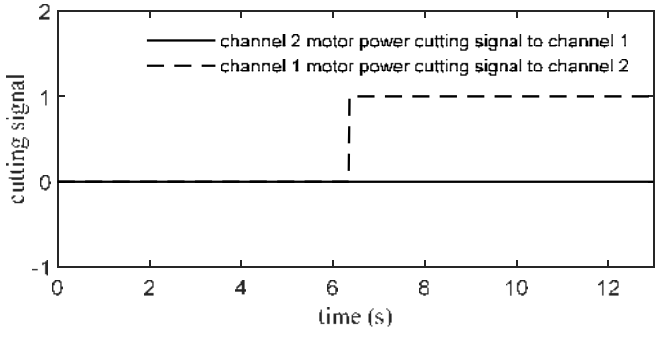

In Figure 31, the information that channel 1 motor is cut off is sent to channel 2 controller, so a step occurs in the dashed line. Then channel 2 controller performs control reforming accordingly.

The target currents and actual currents of the two channel motors collected from the two controllers are shown in Figure 32.

Figure 32 Target and actual currents of two channel motors in order-reduce and reforming test

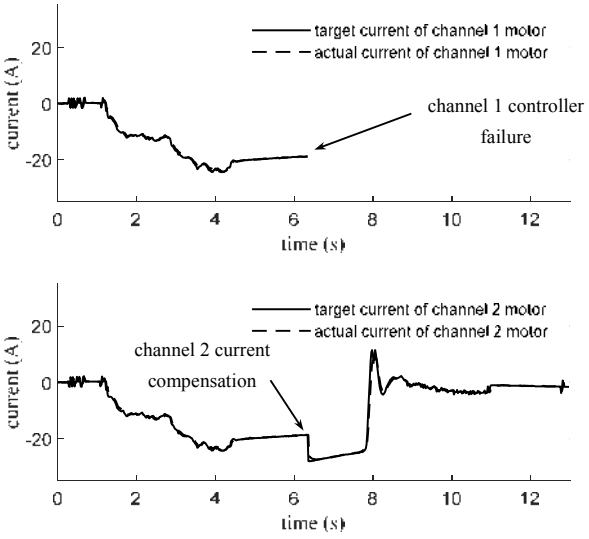

The upper and lower figures in Figure 32 are the target currents and actual currents of channel 1 motor and channel 2 motor. After channel 1 controller fails, its motor current disappears. At the same time, the current of the channel 2 motor has a step there to make up for the torque loss of channel 1 motor.

In order to show that the steering function of the entire system before and after the failure is not affected, the target and actual angle of the steering gear are shown in Figure 33.

Figure 33 Target and actual angles of steering gear in order-reduce and reforming test

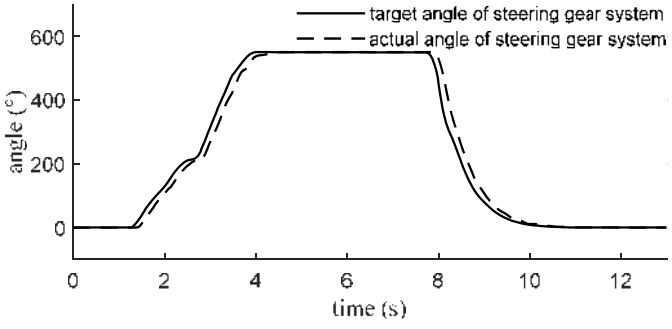

In Figure 33, the actual angle of the steering gear follows the target angle before and after the steering wheel failure occurs, indicating that the vehicle still maintains the steering ability after the failure.

The vehicle test proves that the order-reduce and reforming control method proposed can continue providing the driver with steering torque and maintain steering and aligning function in the case of a single failure. At this time, a fault warning is sent to the driver, so that the system can be repaired in time. This control method is an important part of achieving high safety and reliability of the system.

5 Conclusions

In order to solve the problem of insufficient safety and reliability of the steering wheel system in SBW, a dual-redundancy steering wheel system with high safety and reliability is proposed by this research. This paper proposes a dual-redundancy multi-mode control method for the system.

According to the control method and the vehicle test results, the following conclusions can be drawn.

1 The method proposes different control modes for different vehicle driving needs, which are divided into the angle alignment control when the system is just powered on, the pivot steer with resistance control when the vehicle is stationary and the uniform approaching to middle position control when the vehicle is running. This control method with three modes can basically meet the different driver steering habits during the entire system working cycle, making SBW easier to manipulate.

2 The proposed angle alignment control method can align the angles of steering wheel and steering gear when the system is powered on, preparing for the subsequent normal execution of the steering function.

3 The pivot steer with resistance control can provide the driver with a resistance torque opposite to the speed direction when the vehicle is stationary and keep the steering wheel still when it is not turning. At the same time, the resistance torque can be established smoothly and quickly drops to zero after release, so that the driver has a handle feeling closer to the mechanical system.

4 The uniform approaching to middle position control can make the steering wheel always have a tendency to return to the middle position when the vehicle is running. When the driver turns the steering wheel, it provides the driver with a steering torque that can reflect the change of the steering resistance torque on the front wheels. After the driver releases the hands, the steering wheel can be controlled to return to the middle position and the process is smooth and stable.

5 The system is a dual-redundancy system and this paper proposes a dual-redundancy control method for this system. The proposed torque balance control method can maintain the same output torques in the two motors even if the inputs of the two control channels are different.

6 When the motor in one channel is cut off, the proposed order-reduce and reforming control method can control the motor of another channel to continue working and assume all torque output. The driver's road feel is basically unchanged before and after the failure. This control is a key method to achieve high safety and reliability of the system.

References

Anwar, S. and Niu, W. (2014) 'A nonlinear observer based analytical redundancy for predictive fault tolerant control of a steer-by-wire system', *Asian Journal of Control*, Vol. 16, No. 2, March, pp.321–334.

Balachandran, A. and Gerdes, J.C. (2015) 'Designing steering feel for steer-by-wire vehicles using objective measures', *IEEE/ASME Transactions on Mechatronics*, Vol. 20, No. 1, February, pp.373–383.

Cheon, D.S. and Nam, K.H. (2017) 'Steering torque control using variable impedance models for a steer-by-wire system', *International Journal of Automotive Technology*, Vol. 18, No. 2, pp.263–270.

Fankem, S. and Müller, S. (2014) 'A new model to compute the desired steering torque for steer by wire vehicles and driving simulators', *Vehicle System Dynamics*, Vol. 52, Supplement, pp.251–271.

Hayama, R., Kawahara, S., Nakano, S. and Kumamoto, H. (2010) 'Resistance torque control for steer-by-wire system to improve human–machine interface', *Vehicle System Dynamics*, Vol. 48, No. 9, pp.1065–1075.

He, L., Chen, G.Y. and Zheng, H.Y. (2015) 'Fault tolerant control method of dual steering actuator motors for steer-by-wire system', *International Journal of Automotive Technology*, Vol. 16, No. 6, pp.977–987.

Huang, C. and Li, L. (2020) 'Architectural design and analysis of a steer-by-wire system in view of functional safety concept', *Reliability Engineering & System Safety*, Vol. 198, p.106822.

Huang, C., Naghdy, F. and Du, H. (2020) 'Delta operator-based model predictive control with fault compensation for steer-by-wire systems', *IEEE Transactions on Systems, Man, and Cybernetics: Systems*, Vol. 50, No. 6, June, pp.2257–2272.

Junnan, M., Tong, W., Zhikai, C., Xi, C. and Xiaomin, L. (2020) 'Dual-redundancy steering by wire control system with high safety', *Lecture Notes in Electrical Engineering*, Vol. 574, pp.949–967, *Proceedings of China SAE Congress 2018 Selected Papers*.

Kim, S.H. and Chu, C.N. (2016) 'A new manual steering torque estimation model for steer-by-wire systems', *Proceedings of the Institution of Mechanical Engineers, Part D: Journal of Automobile Engineering*, Vol. 230, No. 7, pp.993–1008.

Lee, J., Yi, K., Lee, D., Jang, B., Kim, M. and Hwang, S. (2020) 'Haptic control of steer-by-wire systems for tracking of target steering feedback torque', *Proceedings of the Institution of Mechanical Engineers, Part D: Journal of Automobile Engineering*, Vol. 234, No. 5, pp.1389–1401.

Lei, H., ChangFu, Z., Chengwei, T., Wu, R. and Zhang, T. (2011) 'DC motor fault diagnosis and fault tolerance control method for steer-by-wire car', *Journal of Jilin University (Engineering and Technology Edition)*, Vol. 41, No. 3, May, pp.608–612.

Ma, B., Yang, Y., Liu, Y., Ji, X. and Zheng, H. (2016) 'Analysis of vehicle static steering torque based on tire-road contact patch sliding model and variable transmission ratio', *Advances in Mechanical Engineering*, Vol. 8, No. 9, pp.1–11.

Wang, T., Chen, X., Cai, Z., Junnan, M. and Lian, X. (2018) 'A mixed model to evaluate random hardware failures of whole redundancy system in ISO 26262 based on fault tree analysis and Markovolume chain', *Proceedings of the Institution of Mechanical Engineers, Part D: Journal of Automobile Engineering*, Vol. 233, No. 4, pp.890–904.

Wang, T., Junnan, Mi., Cai, Z., Chen, X. and Lian, X. (2017) 'Vehicle dual-redundancy electronic steering wheel system', *2017 5th International Conference on Mechanical, Automotive and Materials Engineering (CMAME)*, IEEE, pp.183–187.

Xu, F., Liu, X., Chen, W., Zhou, C. and Cao, B. (2018) 'The fractional order PID method with a fault tolerant module for road feeling control of steer-by-wire system', *Mathematical Problems in Engineering*, Vol. 2018, pp.1–12.

Zhang, H. and Zhao, W. (2018) 'Two-way H∞ control method with a fault-tolerant module for steer-by-wire system', *Proceedings of the Institution of Mechanical Engineers, Part C: Journal of Mechanical Engineering Science*, Vol. 232, No. 1, 1 January, pp.42–56.

Zheng, H., Zong, C., He, L. and Wang, X. (2011) 'Road feel design for vehicle steer-by-wire system', *Transactions of the Chinese Society of Agricultural Machinery*, Vol. 42, No. 2, February, pp.18–22.

Zheng, H., Zong, C., He, L. and Wang, X. (2013) 'Road feel feedback control for steer by wire system based on electric power steering', *Journal of Jilin University (Engineering and Technology Edition)*, Vol. 43, No. 1, January, pp.1–5.

Zou, S. and Zhao, W. (2020) 'Synchronization and stability control of dual-motor intelligent steer-by-wire vehicle', *Mechanical Systems and Signal Processing*, Vol. 145, p.106925.